MyTH4 and FERM Have Overlapping and Distinct Roles in the Function of Myo1, a Class XIV Myosin in *Tetrahymena thermophila*

By

Michael Gotesman

A dissertation submitted to the Graduate Faculty in Biology in partial fulfillment of the requirements for the degree of Doctor of Philosophy,

The City University of New York

2011

This manuscript has been read and accepted for the Graduate Faculty in Biology in satisfaction of the dissertation requirements for the degree of Doctor of Philosophy.

Date	Chair of Examining Committee Dr. Ray H. Gavin, Brooklyn College
Date	Executive Officer Dr. Laurel A. Eckhardt
	Dr. Shaneen M. Singh, Brooklyn College
	Dr. Theodore R. Muth, Brooklyn College
	Dr. Chang-Hui Shen, College of Staten Island
	Dr. Selwyn A. Williams, New York City of Technology
	Dr. Christina King-Smith, Saint Joseph's University

Supervising Committee

The City University of New York

Abstract

MyTH4 and FERM Have Overlapping and Distinct Roles in the Function of Myo1, a Class XIV Myosin in *Tetrahymena thermophila*

By

Michael Gotesman

Adviser: Dr. Ray H. Gavin

MyTH4 and FERM are conserved tail domains in myosin classes VII, X, XII, XIV, XV and in MyoG. Myo1, a class XIV myosin in *Tetrahymena thermophila,* contains MyTH4 and FERM. Previous studies have shown that Myo1 localizes to phagosomes, the cytoskeleton, and the macronucleus, and that phagosome trafficking and division of the macronucleus are affected in a *MYO1* knockout. To investigate the roles for MyTH4 and FERM in the function of Myo1, GFP-tagged MyTH4, FERM, and truncated FERM were separately overexpressed in *Tetrahymena*. Actin antibody coprecipitated tubulin, GFP-MyTH4, and GFP-FERM. GFP-MyTH4 and GFP-FERM cosedimented with either exogenous microtubules or exogenous F-actin. GFP-MyTH4

localized to phagosomes and colocalized with antitubulin to intranuclear microtubules. Overexpression of GFP-MyTH4 inhibited the organization of the parallel array of intranuclear microtubules that form prior to division of the macronucleus. Cells that failed to form the parallel array of microtubules did not advance in nuclear division. Overexpression of GFP-MyTH4 did not affect phagosome recycling. Overexpressed GFP-FERM localized to phagosomes, cytoskeleton, and intranuclear puncta and did not affect division of the macronucleus. Overexpression of truncated GFP-FERM did not localize to the cytoskeleton or nucleus and led to the accumulation of phagosomes at the membrane recycling site in the posterior of the cell. It is unlikely that the overexpression phenotypes are nonspecific effects of GFP. Localization of GFP-fusions is consistent with the localization of full-length Myo1, and overexpression phenotypes mimic the knockout phenotype. Furthermore, GFP-MyTH4 from Myo9, another *Tetrahymena* myosin, did not localize in *Tetrahymena thermophila*. We conclude that MyTH4 and FERM have overlapping roles as indicated by the interaction with actin and tubulin. However, MyTH4 and FERM appear to have distinct roles in the function of Myo1. MyTH4 affects the organization of microtubules involved in macronuclear division, whereas FERM affects recycling of phagosomes and is required for localization to the cytoskeleton.

Acknowledgments

I would like to thank my mentor, Professor Ray Gavin, for working with me on this great project. I believe that we work well together and we have achieved significant progress in better understanding how MyTH4 and FERM function in Myo1. I hope that this project will lead to a better appreciation of how protein domains function to serve proteins and thereby lead to a better understanding of living organisms. Dr. Gavin, is a terrific mentor who has created a wonderful environment in his lab to study and grow as a researcher. I would also like to acknowledge that during my ten years in the Gavin lab, I have learned many important life lessons from my mentor, in terms of day-to-day décor and I developed an overall life perspective. I believe that our relationship has blossomed from mentor/student, to friends, and now something even more special. The amazing microscopy was achieved by Roland Hosein Jr., who has been a much-appreciated asset to my development. He has always been kind and helpful in the lab and I greatly appreciate it. Many technical lab skills were taught to me by Roland, and Kester Hayes.

I would like to also thank Brooklyn College, where I earned my undergraduate degree and performed my graduate work. Brooklyn College has provided me with a home for research and financial support during my graduate education. I would also like to thank members of my Examination Committee, Dr. Selwyn Williams for taking me under his wings, Dr. Shaneen Singh for helpful discussions about MyTH4 domains, Dr. Theodore Muth for many helpful suggestions, and Drs. Chang-Hui Shen and Christina King-Smith for agreeing to serve on my committee. I have also had help from undergraduates during my graduate work, including the brother of Dr. Jorge Garces who cloned the MYO1 gene, Jonathen Garces, Gabriel Lutz, Nalini Seenath and Jesse Flores

and I would like to thank them for laboratory assistance. I would like to acknowledge that I learned much from the faculty and staff at Brooklyn College, including David Klein. My parents have constantly supported me, and I would not have been able to achieve my success without their love and support. Preliminary reports on this research were presented at the 48-50th Annual Meetings of the American Society for Cell Biology, and at the 2010 Pennsylvania Muscle Institute Symposia.

Table of Contents

List of Figures

List of Tables

Chapter 1 Myosin Structure and Function

1.1 Discovery of Myosin

Myosin was first isolated and described by Willi Kuhne in 1864, as a "*proteid"* found in the extracts of frog leg muscles and was later isolated from rabbits (Halliburton, 1887). The role of myosin in muscle contraction led to several very important observations. Myosin was shown to be an ATPase (Engelhardt and Lyubimowa, 1939). Straub isolated the activator of myosin and named it actin for its ability to activate the ATPase catalytic ability of myosin (Straub, 1942; Straub, 1943). Magnesium ion was also shown to be involved in myosin ATPase activity by Banga and et al., (Banga, 1942; Banga and Szent-Gyorgi, 1942). The sliding filament model for muscle contraction explained the role of myosin and actin in muscle contraction (Huxley, 1954). Ultimately, the discovery of a non-conventional or non-filament forming myosin in *Acanthamoeba castellani* (Pollard and Korn, 1973) ushered in the study of non-conventional myosins.

1.2 General Organization of Myosins

The super-family of myosin consists of ~35 classes, with ~2,300 members grouped according to homology in their motor domains (reviews, Berg et al., 2001; Williams and Gavin, 2005; Richards and Cavalier-Smith, 2005; Foth et al., 2006; Ordronitz and Kollmar, 2007). All myosins are actin-dependent molecular motors that utilize the power released in the hydrolysis of ATP to translocate along actin "tracks" (Lymn and Taylor, 1971) in a process known as acto-myosin mediated translocation. Myosins are usually composed of two domains. The N-terminus or motor domain is a highly conserved region among myosins. It has the site for ATP hydrolysis and a site for actin binding, (see review, Gavin, 2001). The C-terminus or tail domain varies greatly

among myosins. The conventional or filament forming myosins are categorized as class II myosins. The unconventional or non-filament forming myosins make up the other ~34 super-classes (Richards and Cavalier-Smith, 2005). Class II myosins have long segments of coiled-coil (CC) regions in their tails. This allows them to form thick filaments as seen in muscle-cells. Because conventional myosins dimerize through their CC domain, many class II myosins can work together to exert a large amount of force as in muscle flexing. Non-filamentous forming myosins (Pollard and Korn, 1973) usually have truncated tails. Unconventional myosins have several other types of domains in their tails that allow myosins to function in specialized cellular activities, such as intracellular trafficking (Durbach et al., 1996, Barsoum and King-Smith, 2007), intranuclear trafficking (Chuang et al., 2006), and to function in mammalian motile and sensory cilia (Wolfrum et al., 1998).

1.3 What are the Different Myosin Homology Tail Domains?

It is presumed that the differences in the myosin tail domain allow myosins to be utilized in a great diversity of function. Class I myosins localize to the leading edge of the lamellipodial projections of migrating *Dictyostelium* amoeba (Fukui, 1989) and to *Acanthamoeba* lipids (Adams and Pollard, 1989) that are transported in vitro along actin tracks (Adams and Pollard, 1986). *Acanthamoeba* class I myosins (Pollenz, 1992) contain three distinct myosin tail domains termed tail homology (TH) regions TH-1, TH-2 and TH-3 (Lee et al., 1999). The TH-1 domain is basic and binds lipids (Doberstein and Pollard, 1992); the TH-2 region is Gly/Pro/Ala-rich (GPA) and binds actin (Lee et al., 1999; Yu and Bement 2007); and the TH-3 region has a 55-residue src homology-3 domain that binds to the PXXP region of the Acan125 protein (Xu et al.,

1997). MyTH4 (myosin-tail-homology-4) (Chen et al., 1996) domain is often coupled with band 4.1-ezrin-radixin-moesin (FERM) as in myosins VII, X, XV (Bohil et al., 2006), XIV (review, Williams and Gavin, 2005), and in the N-terminus of KCBP (kinesin-like-calmodulin-binding protein) (reviews, Berg et al., 2001; Richards and Cavalier-Smith, 2005).

1.4 MyTH4 Domain

MyTH4 is usually adjacent to a FERM domain, although two of the *Tetrahymena* myosins contain either a MyTH4 or FERM but not both (Williams and Gavin, 2005), and in class IV and class XXIII myosins, MyTH4 exists without FERM (Coluccio, 2008). MyTH4 in a kinesin exists independent of FERM (Narasimhulu and Reddy, 1998), and FERM exists independent of MyTH4 in a kinesin-like protein (Awan et al., 2004) and in ERM (ezrin, radixin, moesin) family proteins (Reviewed by Bretscher et al., 2002). Distinct functions for the two domains have generally not been established, and MyTH4/FERM is often described as a single functional complex with actin and tubulin-based roles. Relatively few studies focus on the role of one domain independent of the other. MyTH4 in a plant kinesin directly binds to microtubules (Narasimhulu and Reddy, 1998), but in Myosin X, both MyTH4 and FERM are required for maximal microtubule association (Weber et al., 2004).

1.5 FERM Domain

The founding member of the FERM superfamily, protein 4.1-band, was first recognized as an isolate that acted in the linking of the erythrocyte membrane proteins with spectrin and actin. Protein 4.1-band has been isolated from many other tissues and organs such as the bone marrow, cerebellum, lungs, testes and thymus (Conboy et al.,

1986; review, Diakowski, 2006). Members of the FERM superfamily now include: protein 4.1 band, talin, merlin, protein-tyrosine-phosphatase (PTPH), novel band 4.1-like-4 (NBL4), and ezrin-radixin-moesin (ERM). (review, Diakowski, 2006). The x-ray crystallography of highly conserved ERM proteins, human moesin, shows that the FERM domain forms a compact clover-leaf shaped structure made of three different lobes (1-3) each showing similarity to known structures: ubiquitin, acyl-CoA-binding protein, and the pleckstrin-homology (PH)/ phosphotyrosine-binding (PTB)/ enabled-VASP-homology-1 (EVH1) domain, respectively (Pearson, et al, 2000). Similarly, the x-ray crystallography of mouse merlin revealed that the FERM domain also forms a cloverleaf structure that consists of the previously described lobes (Shimizu et al., 2002).

Several proteins contain a FERM (band 4.1-ezrin-radixin-moesin homology) domain that interacts with the actin and microtubule cytoskeleton (Bretscher et al. 1997; Chishti et al., 1998; Mattagajasingh, 2000; Muranen et al., 2007; Yan, 2001). ERM family proteins consist of an N-terminal FERM domain, an alpha helical domain, and a C-terminal ERM association domain (C-ERMAD) (Reviewed by Bretscher et al., 2002). Each of the three domains contains one or more binding motifs for intramolecular or intermolecular associations (Hamada et al., 2000; Li et al., 2006; Pearson et al., 2000). Structural studies of the FERM domain reveal three sub-domains (F1, F2, F3 or A, B, C) that are potential binding surfaces for proteins, peptides or phospholipids (Pearson et al., 2000; Kitano et al., 2006). In vitro, FERM binds to actin (Lee et al., 2004), tubulin (Muranen et al., 2007), membrane proteins (Yonemura et al, 1998), and phospholipids (Niggli et al., 1995; Hamada et al., 2000). Studies of the interaction between adhesion proteins and ERM proteins reveal that in vivo, ERM proteins exist in either an active or

inactive form. In the inactive or masked state, FERM binds intra-molecularly to the C-ERMAD, an interaction that partially blocks the FERM surface effectively masking binding sites within FERM (Pearson et al., 2000). Unmasking or activation of ERM proteins involves phosphorylation of the tail domain and lipid binding, which release FERM from its intra-molecular binding and unmask binding sites (Hamada et al., 2000; Pearson et al., 2000). Crystal structures of radixin show that FERM bound to the adhesion molecule ICAM-2 (Inter-Cellular Adhesion Molecule) recognizes the C-ERMAD sequence RxxTYxVxxA (Hamada et al., 2003). Crystal structures of moesin reveal another binding site within FERM. Binding of moesin to EBP50 (ezrin binding protein) is prevented in dormant moesin in which FERM binds to a conserved 11-aa (TKQRIDEFEAL) motif in the C-ERMAD. In the active state, moesin FERM binds to the same 11-aa motif in EBP50 (Finnerty et al., 2004). Crystal structure of dimerized radixin FERM domains reveals that the C-terminal conserved motif (KxxTIxVxxM) in one FERM molecule binds sub-domain C within the other FERM molecule (Kitano et al., 2006). Studies of liposomal membranes demonstrate that ERM family proteins (such as talin, 4.1 and ezrin) destabilize membranes and induce large holes in the membrane bilayer (Saitoh et al., 1998; Takeda et al., 2006). Membrane hole formation preferentially occurs with neutral and acidic phospholipids, is reversible, and involves both FERM and the C-terminus of ERM family proteins (Saitoh et al., 1998; Takeda et al., 2006).

One of the 4.1 isoforms termed 4.1R is a mitotic microtubule associated protein and has been shown to partially co-localize with tubulin (Huang et al., 2004). The 30-kDa N-terminus membrane binding domain of 4.1R, termed FERM, is involved in intramolecular interactions with other members of FERM (Pérez-Ferreiro, 2006). Using a

yeast two-hybrid assay, two isoforms (~135 and ~150 kDa) of 4.1R have been shown to interact with actin at tight junctions (Mattagajasingh et al., 2000). Ezrin and its homologs, radixin, moesin, and merlin are concentrated in microvilli and can interact with F-actin to link microfilaments to membrane (Bretscher et al., 1997). Merlin binds to microtubules and actin through its FERM domain (Xu and Gutman, 1998; Taru et al., 2007).

TalinA is another of the FERM proteins that has the FERM N-terminus extension, it has been shown to link the actin cytoskeleton to beta-3-integrin cytoplasmic domains (Yan et al., 2001) and to interact with a previously uncharacterized region of Myosin VII in *Dictyostelium* (Tuxworth et al., 2005). The actin-binding sequence in talin FERM has been elucidated in humans, mouse, *Dictyostelium* and other model organisms (Lee et al., 2004).

1.6 What is Known About the Function of MyTH4/ FERM Coupling in Myosins?

The precise function of MyTH4/FERM coupling is poorly understood, but it is believed to act as a "cross bridge" for microtubule and microfilament interaction either through direct contact or the recruitment of protein partners that can interact with both cytoskeletal proteins (Reddy and Reddy, 1999). A yeast two-hybrid assay showed that Shroom2, an F-actin binding protein, binds to the FERM domain of myosin VIIa (Etournay, 2007).

Human myosin VII contains MyTH4/FERM coupled twice and mutations to this myosin causes Usher Syndrome as well as deafness (Wolfrum et al., 1998). Myosin VIIA is also localized to mammalian cochlear stereocilia (Hasson et al., 1997) and is necessary for *Drosophila* auditory organ development (Todi et al., 2008). A MyTH7 (myosin-tail-

homology-7) domain has been identified as a conserved region in the third lobe of the cloverleaf structure in both FERM domains of myosin VII (Kiehart et al., 2004) and binds actin (Yang et al. 2009).

Myosin X is required for nuclear anchoring and spindle assembly in *Xenopus* oocytes (Weber et al., 2004). Myosin X binds to microtubules through its MyTH4/FERM domain (Weber et al., 2004). The MyTH4/FERM coupled domain in class X myosin also participates in the formation of dorsal filopedia in Hela Cells (Bohil et al., 2006). The FERM domain of myosin X can reorganize F-actin in COS-1 cells (Yonezawa, 2003). The tail region of myosin X post IQ recognizes fascin bundled actin-filaments (Nagy and Rock, 2010).

Mutations to myosin XVa cause deafness in humans and mice, and shakers syndrome in mice. Myosin XVa localizes to the tips of cochlear and vestibular hair cell stereocilia in mice and is necessary for the proper formation of staircase-like arrangement of stereocilia in mature hair bundles (Belyantseva et al., 2003). Myosin XVa is required for programmed stereocilia elongation (Belyantseva et al., 2005). Sisyphus, the *Drosophila* myosin XV homolog, contains an additional MyTH4 in conjunction with a MyTH4/FERM coupled domain that is required for trafficking of alpha-tubulin and tubulin-associated proteins such as Katanin-60, EB1, and Milton (Liu et al., 2008). RNAi knockdown of sisyphus disrupts the organization of both the actin and microtubule cytoskeletal (Liu et al., 2008). Although Myosin V does not contain a MyTH4/FERM coupling, immunofluorescence staining with antibodies against myosin Va revealed localization to microtubule rich regions such as the microtubule organizing center and to the mitotic asters, spindle, and the mid-body of dividing cells in a variety of cell types,

including primary and immortal mouse melanocytes and fibroblasts, Hela cells, and Cos cells (Wu et al., 1998). MAX-1 is a neuronal guidance protein, conserved among drosophila and humans. MAX-1 has a MyTH4/FERM domain and the FERM domain is required for the proper localization of MAX-1 (Huang et al., 2002).

1.7 MyTH4 and FERM Domains in Kinesins

The MyTH4 domain in the C-terminus of an *Arabidopsis* KCBP binds to microtubules (Reddy and Reddy, 1999; Narasimhulu, 1998). A kinesin II kinesin-like-protein (Klps), kin5, in *T. thermophila* has a FERM domain in its tail and localizes to components of the intraflagellar transport system (Awan et al., 2004). The authors speculate that the Kin5 FERM interacts with membrane proteins (Awan et al., 2004).

1.8 Myosin in the Nucleus?

Initial fluorescence recovery after photobleach (FRAP) experiments suggested that the role for actin and myosin in nuclear transport was in controlling the pore size of the nuclear pore complex (Schindler and Jiang, 1986). Class I myosins target the nucleus by an N-terminus extension (Pestic-Dragovich et al., 2000), localize to active nucleoli in human cells, interact with RNA polymerase I complex (Percipalle et al., 2006), and play a role in transcription activation with actin (Ye et al., 2010). Nuclear Myosin I localizes to dense fibrillar component sites of active Pol I transcription and rDNA processing in contrast to nuclear actin which predominately reside in Fibrillar Centers, sites of of Pol I and transcription storage. (Philimonenko et al., 2010, and reviews within). One of the three class V myosin paralogs, Myo5a, localizes to active DNA transcriptional regions in the nucleus (Pranchevicius et al., 2008), termed speckles, and has been implicated in trafficking mRNA from the nucleus to cytosolic destinations (Salerno et al., 2008). The

globular tail of myosin Vb fused to a GFP-tag localized to active transcriptional regions of the nucleus, termed nucleoli, in Hela cells (Lindsay and McCaffrey, 2009). Accordingly, myosin Vb has been shown to interact with beta-actin and RNA polymerase I by coimmunoprecipitation studies (Lindsay and McCaffrey, 2009). A class V myosin in *Saccharomyces cervisiae*, Myo4p is involved in transporting mRNA of ASH1 in cell determination (Chartland and et al., 2002). The Myo16a tail and may target the nucleolus by ankryin repeat domains and colocalizes with actin, and cyclin A in the nucleus (Cameron et al., 2007).

1.9 Myosin Function in Regulating Actin Dynamics

Actin dynamics can be used by cells for intracellular trafficking (Basciano and King-Smith, 2002; McNeil et al., 2004). Filopodia and lamellipodia are cytoplasmic protrusions that contain actin bundles. Myosin-X (Myo10) is ubiquitously expressed in human cells, and localizes at sites of dynamic actin and actin-rich ruffles at the tips of lamellipodia in an actin-independent manner (Berg et al., 2000). Over-expression of GFP-Myo10 in mouse intraembryonic endothelial cells (MECs) increases the number of filopodial extensions (Pi et al., 2007). The tail region of myosin-X, that is C-terminal to the IQ domain, recognizes fascin bundled actin-filaments (Nagy and Rock, 2010). Myo10 colocalizes with Mena/VASP and interacts with the Mena/VASP complex to promote actin growth at filopodia tips in Hela cells (Tokou and Ikebe, 2004). Myo10 initiates filopodia formation as a dimerized motor truncated for the MyTH4/FERM region in COS7 and NIH3T3 cells (Tokou et al, 2007). Interestingly, the MyTH4/FERM domain of Myo10 binds to NPXY in integrins (Zhang et al., 2004).

1.10 Interaction among Microtubules and Actin-filaments

Reviews for complementary (Langford, 1995) and synergistic (Gavin, 1997; Gavin, 1999) roles for microtubule and filamentous actin have elucidated but have not fully explained the mechanism of the interactions between the microtubule and f-actin cytoskeletal polymers. Viscometry experiments in 1978 first revealed actin filament-microtubule interaction mediated by microtubule-associated-proteins (MAPs) (Griffith and Pollard, 1978). Bovine brain derived microtubule-associated-proteins-2 (MAP-2) co-sediments Rabbit psoas (psoas is muscle from the abdomen) actin in a ratio of ~1 molecule of MAP-2 to 28 molecules of actin (Sattilaro et al., 1981). Affinity chromatography and electron microscopy studies have shown that the tubulin binding sequences of tau (Lewis et al., 1988), which is similar to the MAP-2 tubulin binding sequence (Lewis et al., 1988; Doll et al., 1993), binds actin (Correas, et al., 1990). Microscopy and co-sedimentation assays have shown that the previously described actin-binding domains in FERM bind tubulin in ezrin and its homolog in merlin (Muranen et al., 2007). The actin based molecular motor, myosin-Va, has been shown by microscopy and co-sedimentation assays to mechanochemically couple MTs to actin filaments (Cao et al., 2004).

Chapter 2 *Tetrahymena thermophila*

2.1 Culture and Feeding

Tetrahymena thermophila, formerly known as *T. pyriformis* variety 1 or syngen 1 (Nanney and McCoy, 1976), is a free living, heterotrophic, ciliated protist that has been adopted as a model organism for the study of many cellular processes. The oral apparatus (OA) of *Tetrahymena* is a large cortical feeding structure, consisting of ciliated basal bodies (Gavin, 1980). Tubulin (Williams, 1986; Williams and Honts, 1987), actin (Hirino et al., 1987; Hoey and Gavin, 1992; Hosein et al., 2005), myosin (Garcés et al., 1995), and centrin (Guerra et al., 2003) localize to the OA of *T. thermophila*. Phagosomes form in the OA, at the base of the buccal cavity (Kitajima and Thompson, 1977). Cytochalasin B, is an inhibitor of actin polymerization and has been shown to disrupt phagocytosis process in *Tetrahymena,* including the area around the OA (Hoffmann et al., 1974). *Tetrahymena* can grow in the absence of phagocytosis (Rasmussen and Orias, 1975) by utilizing clathrin-dependent endocytosis (Elde et al., 2005). Endocytosis occurs at membrane sites adjacent to cilia, including cilia that compose the oral apparatus (Nillson and Van Deurs, 1983). Phagosomes and endosomes fuse with lysosomes (Kitajima and Thompson, 1977). Of the 73 putative *Tetrahymena* phagosome proteins identified, 28 have been implicated in the phagocytosis process in other organisms (Jacobs et al., 2006). After food is processed in phagosomes, unwanted material is released back to the environment and the surrounding membrane is recycled at the cytoproct, a membrane structure located in the posterior of the cell (Kitajima and Thompson, 1977; Allen and Wolf, 1979). Actin localizes to the cytoproct and treatment of *Tetrahymena* with Latrunculin B disturbs the shape of the cytoproct, however treatment with Nacodozole, a

microtubule depolymerizing agent, inhibits the egestion of food vacuoles through the cytoproct (Sugita et al., 2009)

2.2 Nucleus

Tetrahymena thermophila exhibits nuclear dimorphism; it has a somatic macronucleus (MAC) and a germline micronucleus (MIC). The MAC contains ~45 copies of each chromosome and is active during vegetative growth. The MIC has five chromosomes and is only active during sexual reproduction. During vegetative growth the MAC elongates and constricts, and its contents are divided into two approximately equal subnuclei (Orias, 1991), a process known as amitosis. Amitosis involves the macronuclear microtubules (Williams and Williams, 1976), without much chromosomal condensation in the MAC (Flickinger, 1965). During cytokinesis, cytoplasmic and macronuclear microtubules respectively organize in the cytoplasm and the MAC to aid in macronuclear division (Numata et al., 1999). The *Tetrahymena* macronucleus genome was sequenced (Eisen et al., 2006) and has been open to the public as of 2/2/04 at the *Tetrahymena* Genome Database (ciliate.org). The micronucleus divides mitotically, and two G-DNA-binding proteins, TGP1 and TGP2, aid in micronuclear division (Lu and Henderson, 2000).

2.3 Conjugation

Tetrahymena thermophila is sexually active, having 7 different mating types controlled by the mat locus, which is adjacent to the ribosomal RNA gene (Bleyman, 1992). A zygotic nucleus forms through fusion of a pronucleus from each conjugant. The zygotic nucleus develops into two new genetically matched macronuclei and micronuclei, and the pre-existing macronucleus is eliminated. The first cell division of exconjugants

produces cells with a genetically matched macronucleus and micronucleus.

2.4 Overexpression Vector for Tetrahymena

Ribosomal DNA (rDNA) based vectors (Tondravi and Yao, 1986; Yao, 1986) are used to transform *T. Tetrahymena* (Gaertig et al., 1994) by inducing the amplification of engineered rDNA constructs. pIGF-1, created by M.C. Yao, is commonly used for the over-expression of genes in *Tetrahymena*. The pIGF-1 cloning site consists of an MTT1 promoter (Shang et al., 2002) that is inducible by ionic cadmium, a GFP gene, and a transcriptional stop sequence. The vector also contains *Tetrahymena* and bacterial origins of replication and genes for neomycin and ampicillin resistance. Genes of interest are cloned 3' to the GFP site in pIGF-1 and therefore are expressed with an N-terminus GFP tag. Biolistic bombardment (Cassidy-Hanley et al., 1997; Bruns and Cassidy-Hanley, 2000) is used to insert the vector into *Tetrahymena* mating cells, when they are forming new macronuclei during conjugation. Transformants are selected by antibiotic resistance.

2.5 Cytoskeletal Proteins in T. thermophila

A. Microtubules

Microtubules localize to basal bodies, ciliary axonemes, and other regions of the cortex. The *Tetrahymena thermophila* genome contains genes for one alpha-tubulin (*ATU1*), one gamma-tubulin (*GTU1*), and two beta-tubulin genes (*BTU1* & *BTU2*) (Libisova and Draber 2006). *Tetrahymena* expresses three alpha-tubulin and two beta-tubulin isotypes, three of the alpha isotypes and one of the beta isotype is exclusively found in ciliary microtubules (Suprenant et al., 1985). Gamma-tubulin localizes in vegetative cells to basal bodies (BBs), macronuclear envelopes, micronuclear envelopes, and contractile vacuole pores (Shang et al., 2002).

B. Actin

Act1 is the least divergent of the four *Tetrahymena* actin homologs (Williams et al., 2006). *ACT1* consists of 1128 nucleotides and lacks any introns (Cupples and Pearlman, 1986). The actin protein consists of 375 amino acids, 74% identical to yeast actin and is predicted to have a mass of 42 kDa (Cupples and Pearlman, 1986). *Tetrahymena* actin shares ubiquitous features with its homologs that include polymerization into filaments in the presence of potassium and magnesium ions, and the decoration of heavy mero-myosin (Hirono et al., 1989). Cytochalasin B (Spuddich and Lin, 1972), and Latrunculin A (Coué et al., 1987) are commonly used drugs that inhibit actin polymerization, conversely, phalloidin promotes actin polymerization (Lengsfeld et al., 1974). Phalloidin, however, does not bind to *Tetrahymena* actin (Hirono et al., 1989). Immunobodies raised against a synthetic actin N-terminus peptide localized to the division furrow of dividing cells, as well as the oral apparatus, phagosomes, cytoproct, ciliary meridians and intranuclear microfilament bundles induced by various stresses (Hirono et al, 1987). Immunogold labeled anti-actin localized to actin epitopes in four distinct regions of a filamentous complex that surrounds each basal body in the oral apparatus (Hoey and Gavin, 1992). GFP-tagged actin localized to basal bodies, phagosomes, and cytokinesis-related contractile ring in dividing cells (Hosein et al., 2003). Phenotype of the *ACT1* knockout include: paralysis in motility, arrested cytokinesis, deficiencies in phagosome formation and minor aberrations in ciliary axonemes (Williams et al., 2006). The mRNA levels of *ACT1* is very similar to that of ATU1 (alpha-tubulin) and BTU2 (beta-tubulin).

2.6 Myosin in Tetrahymena

Myo1 is the founding member of the 13 *Tetrahymena thermophila* myosins (Garcés and Gavin, 1998). Myo1 was initially assigned to myosin class XX but more recently re-assigned to a subclass within class XIV (reviews, Berg et al., 2001; Williams and Gavin, 2005; Foth, 2006). The tail of this myosin contains a MyTH4/FERM coupled domain. Myo1 has a mass of 210,889 Daltons and contains 1809 amino acids that include an 89 amino acid N-terminus extension to the 756 amino acid motor, a MyTH4 (myosin-tail-homology 4) domain that extends from amino acid 1234 through and including 1376, and a FERM domain that extends from amino acid 1381 through and including 1799. The Myo1 motor contains a putative internal calmodulin-binding site, termed IQ (review, Cheney, 1992; Rhoads and Friedberg, 1997; Gillespie and Cyr, 2002), which begins with amino acid 758 and ends in amino acid 769.

2.7 What is the Function of Myo1 in Tetrahymena thermophila?

Despite the redundancy of 13 myosins in *T. thermophila* a somatic knockout (KO) of *MYO1* in *Tetrahymena thermophila* displays a phenotype (Williams et al., 2000); and in the last 10 years, this KO has enhanced our knowledge in understanding the inner-workings of cellular trafficking in *Tetrahymena* (Hosein et al., 2005; Hosein and Gavin, 2007). Some of the morphological abnormalities in Myo1 mutants include: smaller cytoplasmic to nuclear ratio, defect in macronuclear elongation which probably explains the longer doubling time at 20ºC, and reduced rate of vacuole formation at 20ºC (Williams et al., 2000). In the KO phagosome motility was random in contrast to wild type *Tetrahymena* in which phagosomes moved in a directed manner toward the posterior of the cell (Hosein et al., 2005). A peptide polyclonal antibody targeting the motor

domain of Myo1 localized to phagosomes and the nucleus (Hosein and Gavin, 2007). Some phagosomes trafficked to the macronucleus in a Myo1 dependent manner (Hosein and Gavin, 2007). The authors speculate that trafficking of phagosomes to the nucleus could transport actin and myosin to the nucleus where they function in amitosis (Hosein and Gavin, 2007).

Chapter 3 Objectives and Experimental Design

Objective

An objective of this research project is to determine how Myo1 localizes to microtubule and actin targets within the cell. An additional objective is to determine whether MyTH4 or FERM region is sufficient for localization to Myo1 targets. We also wish to determine whether MyTH4 and FERM have overlapping or distinct roles in the function of Myo1.

Hypothesis

Myo1 is hypothesized to interact with microtubule and actin filament sites through its MyTH4/FERM coupling. MyTH4 and FERM are hypothesized to bind to MT and AF, respectively. MT-linked MyTH4 and AF-linked FERM are hypothesized to synergistically direct Myo1 to its targets.

Experimental Approach & Design

The general experimental approach was to create truncations of Myo1 that contain various regions of the MyTH4/FERM coupling. The truncated myosins were expressed in *Tetrahymena*. Expressed truncations were localized by confocal microscopy and analyzed for binding partners by low speed cosedimentation assays, coimmunoprecipation, and coimmunoflorescence.

Chapter 4 MyTH4 and FERM Have Overlapping Functions in Myo1

4.1 Genomic Analysis of Myo1

MYO1 consists of 6,337 base pairs (bp) accession number TTHERM_00112430, is located on positions 101,149 through and including 107,485. *MYO1* has 8 introns that are spliced out to create a 5,430 bp mRNA transcript that includes a TGA stop triplet.

Myo1 has a mass of 210,889 Daltons with a theoretical pI of 8.76. Myo1 contains 1,809 amino acids (Fig 1) that include an 89 amino acid N-terminus extension to the 756 amino acid motor, a MyTH4 (myosin-tail-homology-4) domain that extends from amino acid 1,234 through and including 1,376, and a FERM domain that extends from amino acid 1,381 through and including 1,799. The Myo1 motor contains a putative internal calmodulin-binding site, termed IQ (review, Cheney, 1992; Rhoads and Friedberg, 1997; Gillespie and Cyr, 2002), which begins with amino acid 758 and ends in amino acid 769.

Fig. 1

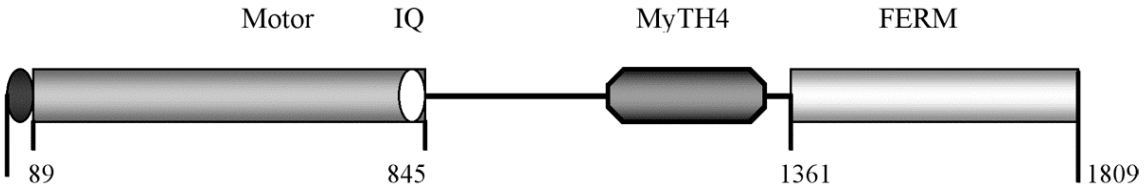

Fig. 1. Myo1, a class XIV myosin. **(A)** Diagram of Myo1. The oval (aa 1-89) represents the N-terminal extension. The location of MyTH4 was determined by prosite (Hulo and et al., 2007). The location of FERM was determined by alignment of the Myo1 tail domain with *Mus* radixin.

4.2 Bioinformatic Analysis of MyTH4 and FERM

To search for possible binding motifs that could form the basis for MyTH4 interactions, MyTH4 was aligned with sequences that involve actin binding, tubulin binding, FERM-FERM interactions and nuclear localization. Lee et al. (2004) identified a cluster of FERM domain amino acids that were proposed to mediate an electrostatic interaction between actin and talin. In the present study we sought to determine whether the same cluster of amino acids exists in MyTH4 and, therefore, represent a putative binding site for actin. The MyTH4 sequence was aligned with the actin-binding site (ABS1) in the N-terminal FERM domain of *Dictyostelium* talinB (Lee et al., 2004) and with one of the four tandem repeats in the tubulin-binding domain of *Rattus* MAP-2 (Doll et al., 1993) (Fig. 2). The talin (ABS) and MAP-2 (TBS) sequences loosely matched two non-overlapping sequences in MyTH4 (Figs. 2A-2B). Alignment of the MyTH4 sequence with (PPKKKRKVED), the nuclear localization sequence (NLS) in Simian virus 40 large T antigen, revealed an NLS-like sequence in MyTH4 (Fig. 2C). Myo1 FERM (Gotesman et al., 2010) contains a sequence that loosely matched a conserved radixin FERM sequence (Kitano et al., 2006) reportedly involved in dimerization of radixin FERM. The alignment in Fig. 2D revealed a similar sequence in MyTH4.

Fig. 2

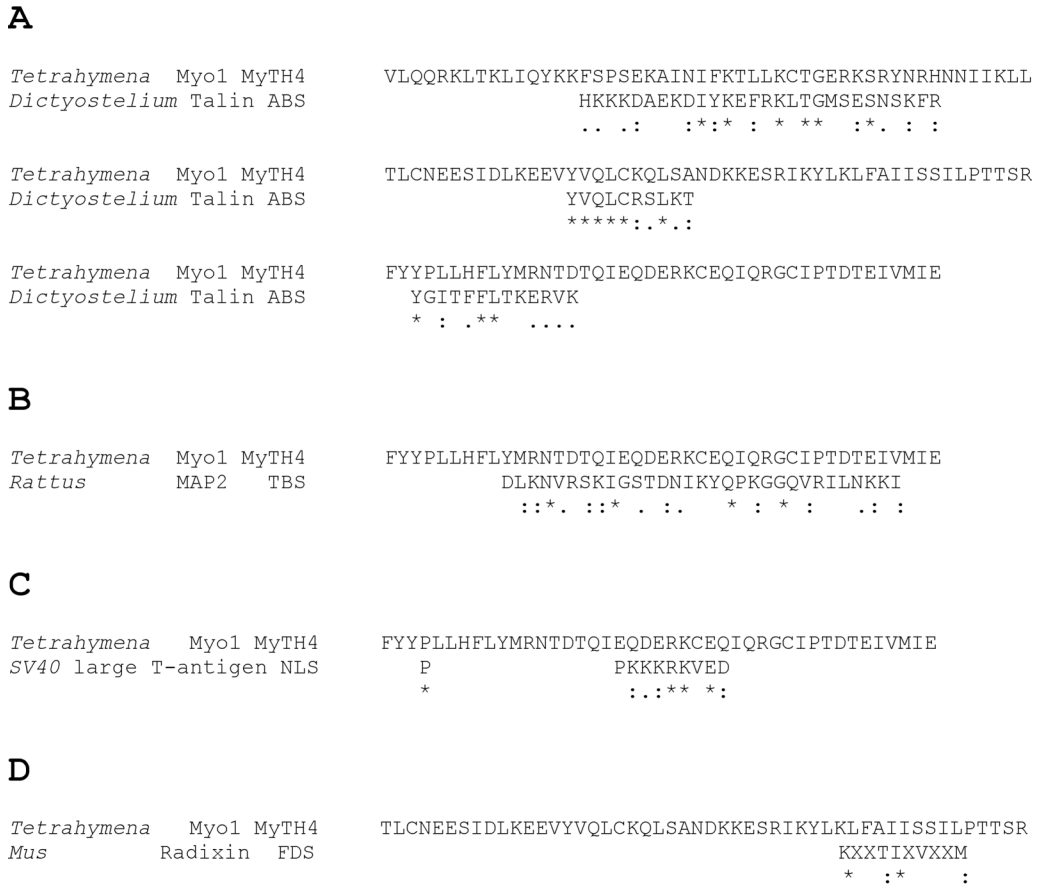

Fig. 2. MyTH4 Clustal W alignments. Portions of the MyTH4 sequence are not shown. **(A)** Clustal W alignment of Myo1 MyTH4 and the actin-binding sequence in the N-terminal FERM domain of *Dictyostelium* talinB. Putative actin-binding sequence in Myo1 MyTH4 (aa 1249-1348): Identities = 15/51(29%), Positives = 36/51(70%). **(B)** Clustal W alignment of Myo1 MyTH4 and the tubulin-binding sequence in *Rattus* MAP-2. Putative tubulin-binding sequence in Myo1 MyTH4 (aa 1343-1373): Identities = 4/31(13%), Positives = 17/31(55%). **(C)** Clustal W alignment of Myo1 MyTH4 with the nuclear localization sequence (PPKKKRKVED) for Simian virus 40 large T antigen. Putative NLS in Myo1 MyTH4 (aa 1337-1360): Identities = 4/10(40%), Positives = 8/10(80%). **(D)** Clustal W alignment of Myo1 MyTH4 and the conserved FERM

putative imerization motif (KxxTIxVxxM) in *Mus* radixin. X= any amino acid. Putative dimerization sequence in Myo1 MyTH4 (aa 1319-1328): Identities = 2/5(40%), Positives = 4/5(80%).

To search for putative binding motifs involving FERM, Myo1 FERM was aligned with the actin-binding sequence (ABS1) in the N-terminal FERM domain of *Dictyostelium* talinB (Lee et al., 2004) and with one of the four tandem repeats in the tubulin-binding domain of *Rattus* MAP-2 (Doll et al., 1993). The talin sequence loosely matched two non-overlapping, putative actin-binding sequences in the N-terminal and C-terminal regions of Myo1 FERM (Fig. 3A). The MAP-2 sequence loosely matched two non-overlapping, putative tubulin-binding sequences in the N-terminal and C-terminal regions of Myo1 FERM (Fig. 3B). The bold face type in Fig. 3A-B indicates amino acids that appear in both actin and tubulin-binding sequences. Alignment of Myo1 FERM with the sequence KxxTIxVxxM, a conserved motif involved in dimerization of FERM in *Mus* radixin (Kitano et al., 2006), revealed a closely matched sequence in the N-terminal region of the FERM domain and another matched sequence in the FERM C-terminal region. Here, the KxxTIxVxxM motif is referred to as the FERM dimerization sequence (FDS) (Fig. 3C). Alignment of Myo1 with the C-ERMAD sequence (TKQRIDEFEAL) (Finnerty et al., 2004) revealed a similar sequence in residues 340-350 in the Myo1 motor domain (Fig. 3D). Alignment of Myo1 with the ERM alpha helical domain sequence (TTPxxxxxxE) (Li et al., 2006) revealed a sequence match in Myo1 residues 1046-1055 C-terminus of the motor domain (not shown). An additional search for binding motifs involved alignment of Myo1 FERM with the nuclear localization sequence

(PPKKKRKVED) for Simian virus 40 large T antigen. Alignment revealed NLS-like sequences in both the N-terminus and C-terminus regions of FERM (Fig. 3E).

Fig. 3.

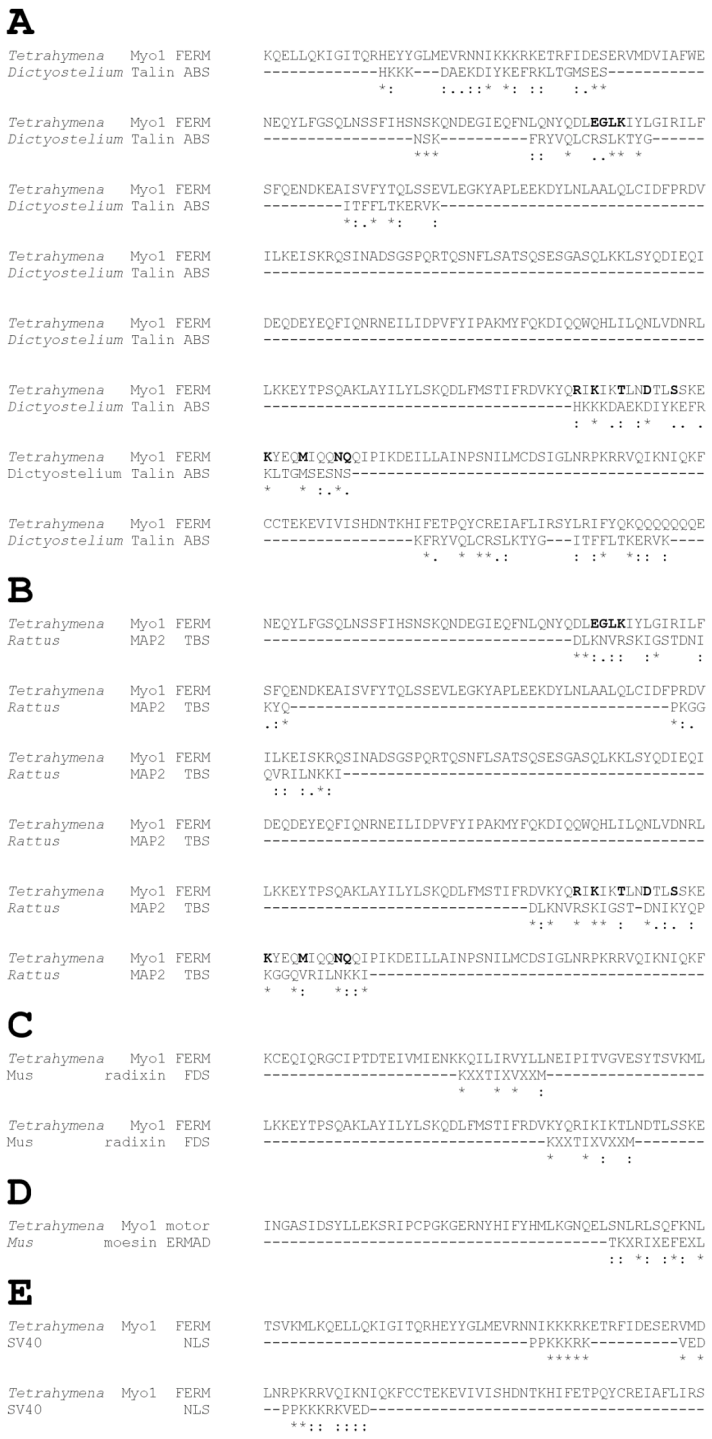

Fig. 3. FERM Clustal W alignments. Portions of the FERM sequence are not shown. **(A)** Clustal W alignment of Myo1 FERM and the actin-binding sequence in the N-terminal FERM domain of *Dictyostelium* talinB. Putative actin-binding sequence in Myo1 FERM N-terminal region (aa 1420-1526): Identities = 15/51(29%), Positives = 34/51(67%). Putative actin-binding sequence in Myo1 FERM C-terminal region (aa 1692-1802): Identities = 11/51(22%), Positives = 29/51(57%). **(B)** Clustal W alignment of Myo1 FERM and the tubulin-binding sequence in *Rattus* MAP-2. Putative tubulin-binding sequence in Myo1 FERM N-terminal region (aa 1492-1565): Identities = 5/31(16%), Positives = 20/31(65%). Putative tubulin-binding sequence in Myo1 FERM C-terminal region (aa 1687-1718): Identities = 10/31(32%), Positives = 19/31(61%). **(C)** Clustal W alignment of Myo1 FERM and the conserved FERM dimerization motif (KxxTIxVxxM) in *Mus* radixin. X= any amino acid. Putative dimerization sequence in Myo1 FERM N-terminal region (aa 1379-1388): Identities = 3/5(60%), Positives = 4/5(80%). Putative dimerization sequence in Myo1 FERM C-terminal region (aa 1689-1698): Identities = 2/5(40%), Positives = 4/5(80%). **(D)** Clustal W alignment of Myo1 motor (aa 340-350) with the conserved C-ERMAD sequence (TKQRIDEFEAL). Identities = 3/11(27%), Positives = 8/11(73%). **(E)** Clustal W alignment of Myo1 FERM with the nuclear localization sequence (PPKKKRKVED) for Simian virus 40 large T antigen. Putative NLS in Myo1 FERM N-terminal region (aa 1431-1450): Identities = 7/10(70%), Positives = 7/10(70%). Putative NLS in Myo1 FERM C-terminal region (aa 1743-1752): Identities = 2/10(20%), Positives = 8/10(80%).

4.3 Putative Binding Motifs in MyTH4 and FERM

Overexpression of GFP-MyTH4 and GFP-FERM in *Tetrahymena thermophila* was used to investigate the role of putative actin and tubulin binding motifs in the function of MyTH4 and FERM (Figs 4 and 5). GFP-MyTH4 and a truncated version of the MyTH4 were separately expressed in *Tetrahymena* (Fig 4). GFP-MyTH4 contained the entire GFP-MyTH4 domain (Fig 4B). GFP-MyTH4T contains the entire MyTH4 sequence N-terminal to the putative TBS (Fig 4C).

4.4 MyTH4 Overexpression Constructs

Fig. 4.

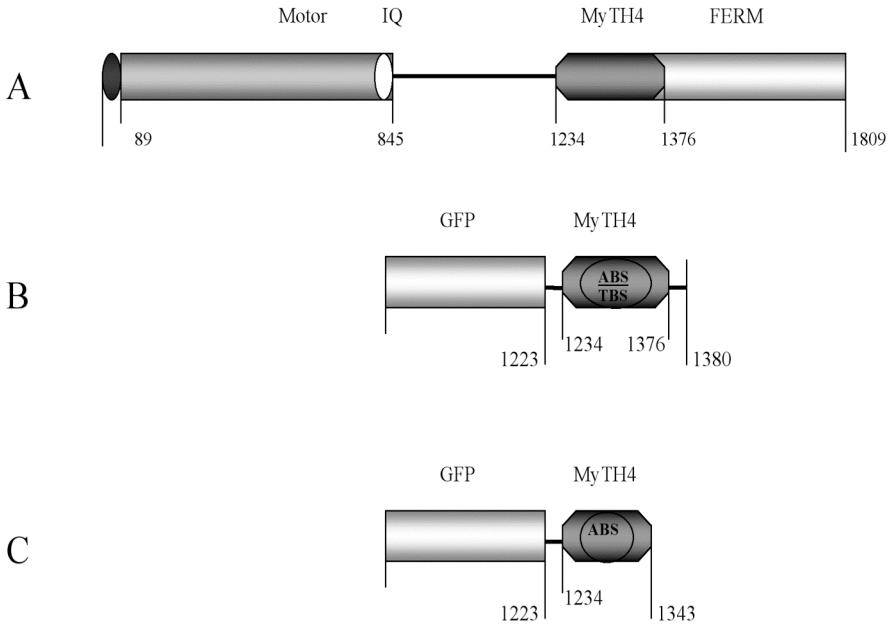

Fig 4. Myo1, a class XIV myosin. **(A)** Diagram of Myo1. The oval (aa 1-89) represents the N-terminal extension. Diagrams of constructs prepared from truncated Myo1-tail domains. **(B)** GFP-MyTH4. **(C)** Truncated GFP-MyTH4. Actin Binding Sequence (ABS) and Tubulin Binding Sequence (TBS) are indicated within the ovals in the diagram.

4.5 FERM Overexpression Constructs

GFP-FERM and two truncated FERM domains derived from GFP-FERM were separately expressed in *Tetrahymena* to test putative binding sequences. GFP-FERM contained the entire Myo1 FERM domain (Fig. 5B). Truncated Myo1 FERM domains contained either the N-terminal or the C-terminal region of FERM and one putative sequence for actin binding, one for tubulin binding, a putative dimerization motif, and a NLS-like sequence.

Fig. 5.

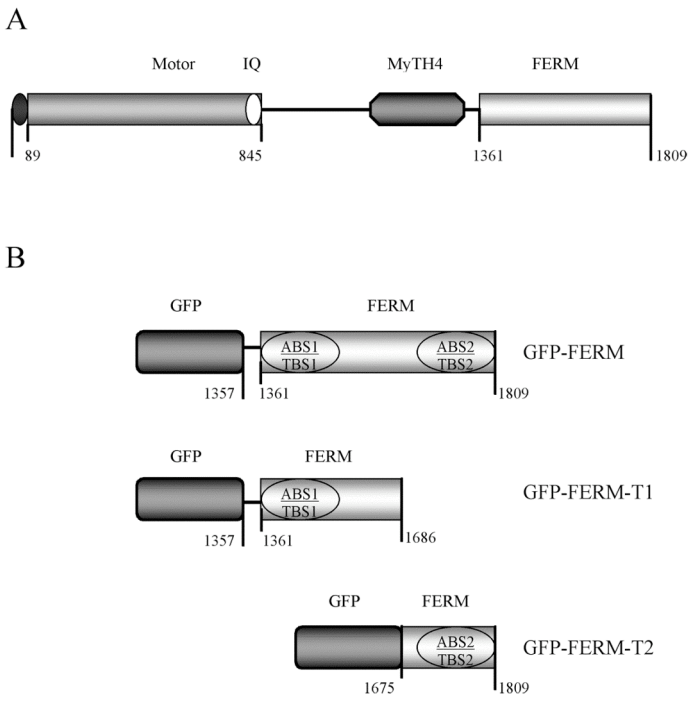

Fig 5. Myo1, a class XIV myosin. **(A)** Diagram of Myo1. The oval (aa 1-89) represents the N-terminal extension. The location of FERM was determined by alignment of the Myo1 tail domain with *Mus* radixin. **(B)** Diagrams of constructs prepared from truncated Myo1-tail domains. Actin Binding Sequence (ABS) and Tubulin Binding Sequence (TBS) are indicated within the ovals in the diagram.

4.6 MyTH4 Overexpression in Transformed Tetrahymena

Expression of GFP-MyTH4 was initiated by addition of cadmium chloride to a population of transformed cells previously grown for 8-12 hours. Over a 12-hr period following initiation of over expression, cell density gradually declined, in sharp contrast to an untreated control population, which remained in exponential phase of growth. To confirm expression of GFP-MyTH4, total cell lysate was prepared from cells approximately 8 hours after induction of overexpression. The lysate was analyzed on an immunoblot probed with GFP antibody, which detected the GFP fusion polypeptide at the expected relative molecular mass of 47 kDa (Fig. 6A).

Fig. 6.

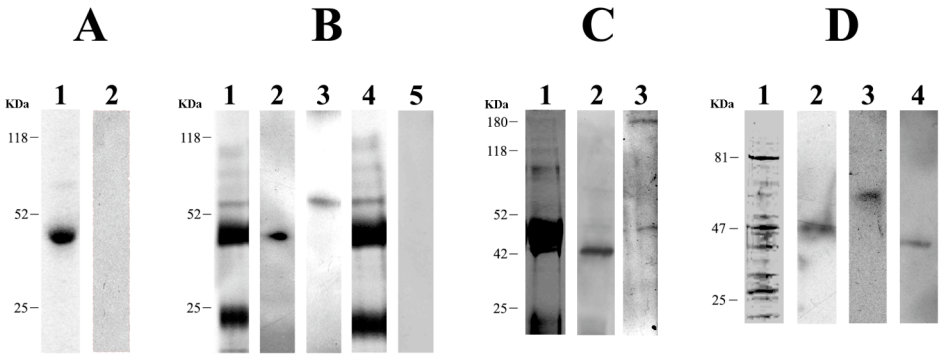

Fig 6. Gel and immunoblot analysis of GFP-MyTH4 overexpressing cells. **(A)** Immunoblot analysis of cells expressing GFP-MyTH4. The blots were probed with mouse antiGFP. Lane **1**: GFP-MyTH4. The fusion protein is 47 kDa. Lane **2**: Wild-type control. **(B)** Gel and immunoblot analysis of antiactin immunoprecipitation pellets (IP) from cells overexpressing GFP-MyTH4. Gel loadings were equal for all lanes. Lane **1**: Gel of antiactin IP from GFP-MyTH4. Lane **2**: Blot of antiactin IP from GFP-MyTH4. The blot was probed with anti-GFP. The fusion protein is 47 kDa. Lane **3**: Blot of

antiactin IP from GFP-MyTH4. The blot was probed with mouse antitubulin. Tubulin is at 55kDa. Lane **4**: Gel of antiactin IP from a strain expressing GFP alone. Lane **5.** Blot of antiactin IP from GFP alone. The blot was probed with mouse antiGFP. **(C)** Gel and immunoblot analysis of antiactin immunoprecipitation pellet (IP) from cells overexpressing GFP-MyTH4. Lane **1**: Gel of antiactin IP from GFP-MyTH4. Lane **2**: Blot of antiactin IP from GFP-MyTH4. The blot was probed with rabbit antiactin. Actin is at 42 kDa. The IgG heavy chain is approximately 50 kDa. Lane **3**: Blot of antiactin IP from GFP-MyTH4. The blot was probed with rabbit antiMyo1. Myo1 is at 180 kDa. The IgG heavy chain is approximately 50 kDa. **(D)** Gel and immunoblot analysis of antiGFP pulldown fraction from cells overexpressing GFP-MyTH4. Gel loadings were equal for all lanes. Lane **1**: Gel of affinity purified GFP-MyTH4 fraction. Lane **2**: Blot of antiGFP pulldown fraction. The blot was probed with anti-GFP. The fusion protein is 47 kDa. Lane **3**: Blot of antiGFP pulldown fraction. The blot was probed with mouse antitubulin. Tubulin is at 55 kDa. Lane **4**: Blot of antiGFP pulldown fraction. The blot was probed with rabbit antiactin. Actin is at 42 kDa.

4.7 Antiactin Antibody Coprecipitates GFP-MyTH4

Clustal alignments indicated a putative tubulin-binding site and a putative actin-binding site within MyTH4. Therefore, to obtain additional evidence that MyTH4 interacts with tubulin and to investigate MyTH4 interaction with actin, non-denatured lysate from a strain expressing GFP-MyTH4 was processed for immunoprecipitation (IP) with antiactin, and precipitated proteins were eluted from ProteinA-agarose beads. Actin antibody coprecipitated GFP-MyTH4, tubulin, actin, and Myo1 (Figs. 6B-6C). The expression level of Myo1 in overexpressing cells appeared comparable to the expression level in wild type. In a control experiment, actin antibody precipitated several proteins from lysate of cells expressing GFP alone, and the control IP gel is quite similar to the GFP-MyTH4 antiactin IP gel (Fig. 6B). However, GFP was not detected on an immunoblot of the control IP (Fig. 6B).

4.8 AntiGFP Affinity Pulls Down GFP-MyTH4, Tubulin, and Actin

For affinity purification of GFP-MyTH4, non-denaturing lysate from the GFP-MyTH4 strain was incubated with antiGFP-linked agarose. The eluted fraction contained several polypeptides including GFP-MyTH4, actin, and tubulin (Fig. 6D). Myo1 was not detected in the eluted fraction.

4.9 GFP-Myo1 Tail Fusions Interact With Actin and Tubulin

To demonstrate that GFP-MyTH4 and GFP-FERM fusions interact with actin and tubulin in vivo, non-denatured extracts from cells over-expressing GFP-fusions were used in low speed co-sedimentation assays with either exogenous phalloidin (Alexa-Fluor 568)-stabilized actin filaments or exogenous rhodamine-labeled microtubules. Phalloidin

does not bind to *Tetrahymena* actin filaments (Hirono et al., 1989), and therefore the assay did not detect endogenous F-actin.

4.10 GFP-MyTH4 Associates With Parallel Arrays of Crosslinked Exogenous Microtubules and Crosslinked Exogenous F-actin

Antiactin IP, antiGFP pulldown fraction, and whole cell extract from the GFP-MyTH4 strain were separately used in low speed cosedimentation assays with either exogenous rhodamine-labeled microtubules or exogenous phalloidin (Alexa-Fluor 568)-stabilized F-actin (Fig. 7). Phalloidin does not bind to *Tetrahymena* F-actin (Hirono et al., 1989), and therefore the assay did not detect endogenous F-actin. To eliminate binding of actin to myosin motor domains, actin cosedimentation assays were performed in the presence of added 10 mM Mg-ATP.

4.11 Cosedimentation Assays of MyTH4 With f-Actin or Microtubules

Examination of the pellet from a cosedimentation assay with microtubules and antiactin IP revealed significant colocalization of green (GFP-MyTH4) and red (exogenous microtubules) fluorescence (Figs. 7B-7D). Examination of the pellet from a cosedimentation assay with labeled F-actin and antiactin IP revealed significant colocalization of green (GFP-MyTH4) and red (F-actin) fluorescence (Figs. 7F-7H). GFP alone did not cosediment with either F-actin or microtubules. Next, we asked whether exogenous F-actin affects microtubule aggregation. A cosedimentation assay was performed with a mixture of unlabeled F-actin, rhodamine-labeled microtubules, and antiactin IP. Microtubules appeared to be more extensively crosslinked in the presence of F-actin (Figs. 7J-7L, Inset). Whole cell extract from the GFP-MyTH4 strain was used in a cosedimentation assay with either exogenous microtubules (Fig. 7N-7P) or exogenous

F-actin (Figs. 7R-7T). Significant colocalization of the two signals was observed in the pellet from each assay. To rule out non-specific aggregation by GFP, a control experiment used F-actin in the presence of 10 mM Mg-ATP and whole cell extract from a strain that expressed GFP alone. Examination of the pellet from the control cosedimentation assay did not detect colocalization of red and green fluorescence as shown in merged red and green channel images (Fig. 7X). The antiGFP pulldown fraction was used in cosedimentation assays with either exogenous microtubules or exogenous F-actin. Figs. 7AA-HH show that the affinity purified GFP-MyTH4 cosedimented with exogenous F-actin and exogenous microtubules, consistent with cosedimentation assays involving antiactin IP. The images of crosslinked F-actin and crosslinked microtubules appear highly similar in assays involving either antiactin IP or the antiGFP pulldown fraction.

Fig. 7.

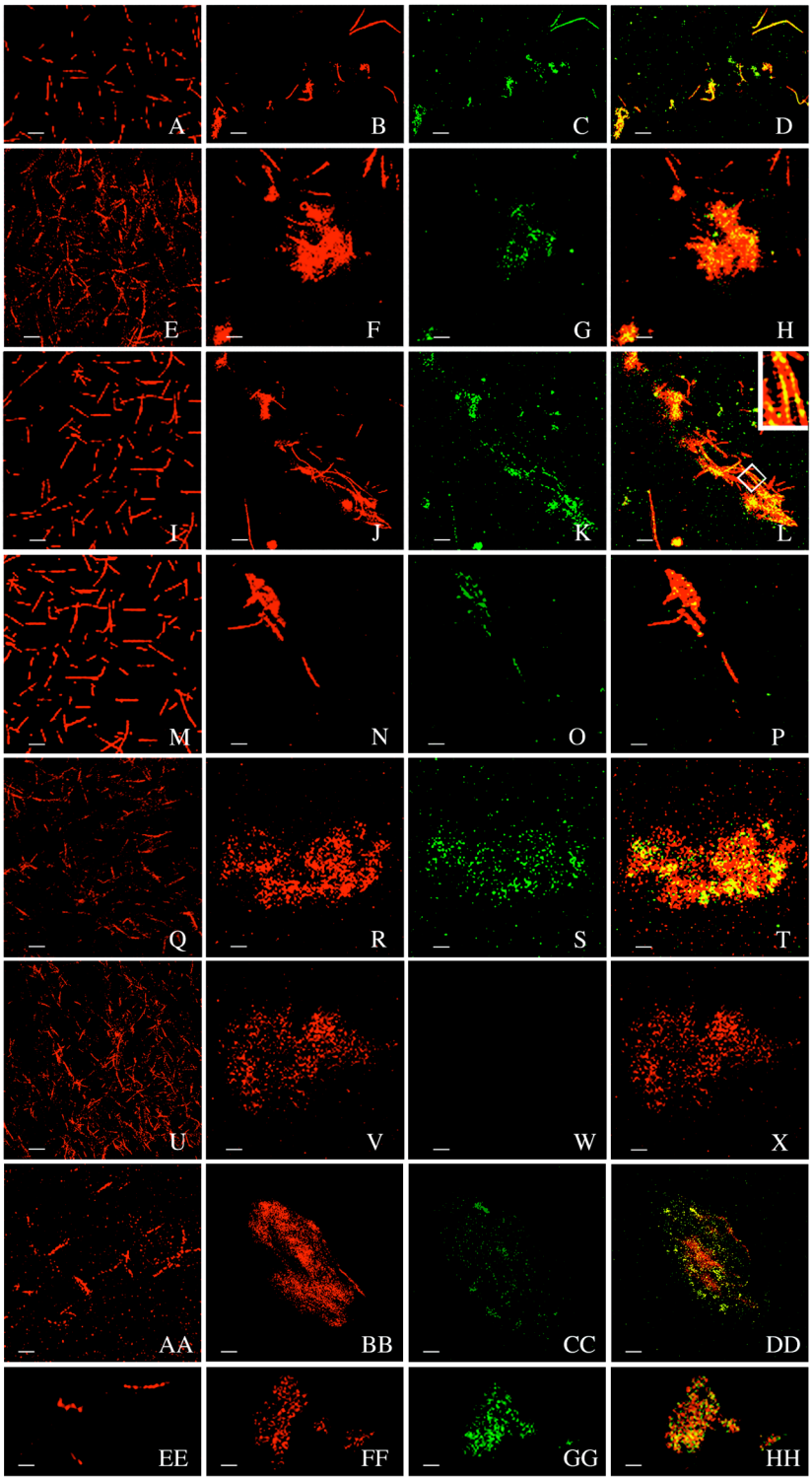

Fig 7. Cosedimentation analysis of GFP-MyTH4 overexpresing cells. Scale bar = 5 μm. (**A-D**) Cosedimentation of microtubules (red) and antiactin IP from GFP-MyTH4 lysate. **(A)** Taxol-stabilized microtubules prior to cosedimentation. **(B-D)** Pellet from cosedimentation of microtubules and antiactin IP. **(B)** Microtubule signal. **(C)** GFP signal. **(D)** Image from merged red-green channels. **(E-H)** Cosedimentation of phalloidin-labeled, muscle F-actin (red) and antiactin IP from GFP-MyTH4 lysate. **(E)** F-actin prior to cosedimentation. **(F-H)** Pellet from cosedimentation of F-actin and antiactin IP. **(F)** F-actin signal. **(G)** GFP signal. **(H)** Image from merged red-green channels. (**I-L**) Cosedimentation of microtubules (red), unlabeled muscle F-actin, and antiactin IP from GFP-MyTH4 lysate. **(I)** Taxol-stabilized microtubules prior to cosedimentation. **(J-L)** Pellet from cosedimentation of microtubules, unlabeled F-actin, and antiactin IP. **(J)** Microtubule signal. **(K)** GFP signal. **(L)** Image from merged red-green channels. The inset shows a higher magnification of a portion of the microtubule cross-linked array. The bar in (**L**) represents 18.5 μm for the inset. (**M-P**) Cosedimentation of microtubules (red) and whole cell extract from GFP-MyTH4 strain. **(M)** Taxol-stabilized microtubules prior to cosedimentation. **(N-P)** Pellet from cosedimentation of Taxol-stabilized microtubules and extract from cells expressing GFP-MyTH4. **(N)** Microtubule signal. **(O)** GFP signal. **(P)** Image from merged red-green channels. (**Q-T**) Cosedimentation of phalloidin-labeled, muscle F-actin (red) and whole cell extract from GFP-MyTH4 strain. **(Q)** F-actin prior to cosedimentation. **(R-T)** Pellet from cosedimentation of F-actin (red) and extract from cells expressing GFP-MyTH4. **(R)** F-actin signal. **(S)** GFP signal. **(T)** Image from merged red-green channels. (**U-V**) Cosedimentation of F-actin and extract from cells expressing GFP alone. **(U)** Phalloidin-

labeled muscle F-actin prior to cosedimentation. **(V-X)** Pellet from cosedimentation of F-actin and extract from cells expressing GFP alone. **(V)** F-actin signal. **(W)** GFP signal. **(X)** Image from merged red-green channels. **(AA-DD)** Cosedimentation of phalloidin-labeled, muscle F-actin (red) and antiGFP pulldown fraction. **(AA)** F-actin prior to cosedimentation. **(BB-DD)** Pellet from cosedimentation of F-actin and antiGFP pulldown fraction. **(BB)** F-actin signal. **(CC)** GFP signal. **(DD)** Image from merged red-green channels. (**EE-HH**) Cosedimentation of microtubules (red) and antiGFP pulldown fraction. **(EE)** Taxol-stabilized microtubules prior to cosedimentation. **(FF-HH)** Pellet from cosedimentation of microtubules and antiGFP pulldown fraction. **(FF)** Microtubule signal. **(GG)** GFP signal. **(HH)** Image from merged red-green channels.

4.12 FERM Overexpression in Tetrahymena thermophila

Expression of GFP-FERM and GFP-FERM truncations was initiated by addition of 0.1- 0.5 µg/ml cadmium chloride to cultures of transformed cells. GFP fluorescence was detected within 2-3 hours after addition of cadmium. Transformed cells that over-expressed GFP-fusion proteins exhibited significantly longer doubling times than wild-type cells. For example, at 0.1 µg/ml cadmium chloride the doubling time for the GFP-FERM strain was 6.8 $\pm$ 2.3 hours in contrast to 3.1 $\pm$ 1.1 hours for wild-type control cells. Cadmium chloride concentrations greater than 0.1 µg/ml induced longer doubling times. At 1.0 µg/ml cadmium chloride there was significant cell death, and exponential growth was not achieved. Lysates from strains that over-expressed GFP-FERM, GFP-FERM-T1, or GFP-FERM-T2 were analyzed on immunoblots probed with GFP antibody, which detected GFP-fusion polypeptides at 80 kDa, 64 kDa, and 45 kDa, respectively (Fig. 7A). GFP-fusion polypeptides were not detected in lysate from a strain over-expressing GFP alone.

Fig. 8.

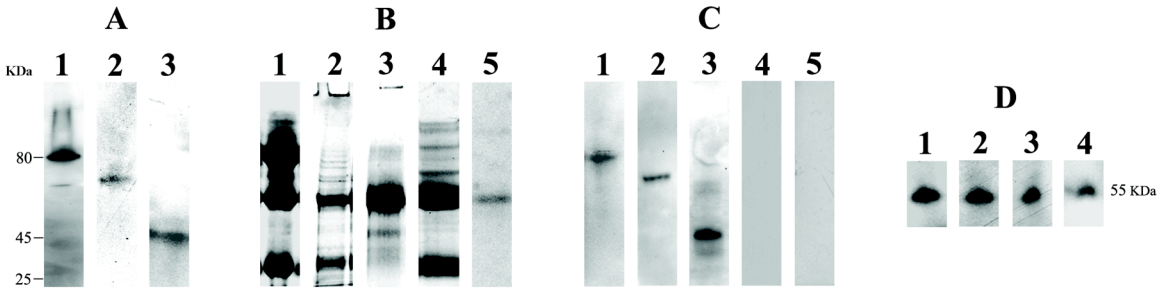

Fig 8. Immunoprecipitation (IP) and Immunoblot analysis of GFP-FERM, and GFP-FERM truncations overexpressing cells. **(A)** Immunoblots of whole cell lysate from GFP-fusion strains. Blots were probed with mouse anti-GFP. Lane **1**: GFP-FERM. The

fusion protein is 80 kDa. Lane **2**: GFP-FERM-T1. The fusion protein is 64 kDa. Lane **3**: GFP-FERM-T2. The fusion protein is 45 kDa. **(B)** SDS-PAGE of anti-actin immunoprecipitation pellets (IP). Gels were stained with Coomassie Blue. Lane **1**: Gel of anti-actin IP from GFP-FERM. Lane **2**: Gel of anti-actin IP from GFP-FERM-T1. Lane **3**: Gel of anti-actin IP from GFP-FERM-T2. Lane **4**: Gel of anti-actin IP from GFP alone. Lane **5**: Gel of rabbit non-immune serum precipitate from GFP-FERM. **(C)** Immunoblots of anti-actin IPs. All blots were probed with anti-GFP.

Lane **1**: Blot of anti-actin IP from GFP-FERM. The fusion protein is 80 kDa. Lane **2**: Blot of anti-actin IP from GFP-FERM-T1. The fusion protein is 64 kDa. Lane **3**: Blot of anti-actin IP from GFP-FERM-T2. The major band is at 45 kDa. Lane **4**: Blot of anti-actin IP from cells expressing GFP alone. Lane **5**: Blot of rabbit non-immune serum precipitate from GFP-FERM. **(D)** Immunoblots of anti-actin IPs. All blots were probed with mouse anti-beta tubulin. Tubulin is 55 kDa in each lane. Lane **1**: Blot of anti-actin IP from GFP-FERM. Lane **2**: Blot of anti-actin IP from GFP-FERM-T1. Lane **3**: Blot of anti-actin IP from GFP-FERM-T2. Lane **4**: Blot of anti-actin IP from GFP alone.

4.13 Antiactin Antibody Coprecipitates GFP-FERM

To provide further evidence that FERM interacts with actin and tubulin in vivo, non-denatured lysate from each strain expressing a GFP-fusion polypeptide was processed for immunoprecipitation with rabbit anti-actin (Fig. 8B). Actin antibody co-precipitated GFP-fusion polypeptides (Fig. 8C) and tubulin (Fig. 8D). Specifically, the immunoprecipitation (IP) pellets contained GFP-fusion polypeptides at 80 kDa, 64 kDa, and 45 kDa from strains expressing respectively, GFP-FERM, GFP-FERM-T1, and GFP-FERM-T2 (Fig. 8C). The IP pellets also contained actin and Myo1 (not shown). Two control experiments were performed to rule out non-specific binding of GFP to actin and other proteins. In one control experiment, an anti-actin IP pellet was prepared from cells expressing GFP alone and analyzed on an immunoblot probed with anti-GFP, which did not detect GFP (Fig. 8C). In another control experiment, GFP was not detected on immunoblots of precipitation pellets obtained with non-immune serum (Fig. 8C).

4.14 Antiactin Immunoprecipitation Pellets Contain GFP-FERM Fusions That Interact With f-Actin and Microtubules

IP pellets were used in co-sedimentation assays with either exogenous F-actin or exogenous microtubules. F-actin and microtubules were randomly distributed prior to use in the assays (Fig. 9A, E). Examination of the pellets from low speed centrifugation revealed co-localization of red and green fluorescence in aggregates of exogenous F-actin (Fig. 9B-D). In parallel assays with exogenous microtubules, examination of co-sedimentation pellets revealed co-localization of red and green fluorescence in aggregates of exogenous microtubules (Fig. 9F-H). To determine whether exogenous actin filaments affect microtubule aggregation, a co-sedimentation assay was performed with a mixture

of unlabeled F-actin, rhodamine-labeled microtubules, and IP pellet. Addition of actin filaments did not appear to affect aggregation of microtubules (Fig. 9G-H). In the presence of GFP alone, actin filaments and microtubules did not sediment at low speed centrifugation.

Fig. 9.

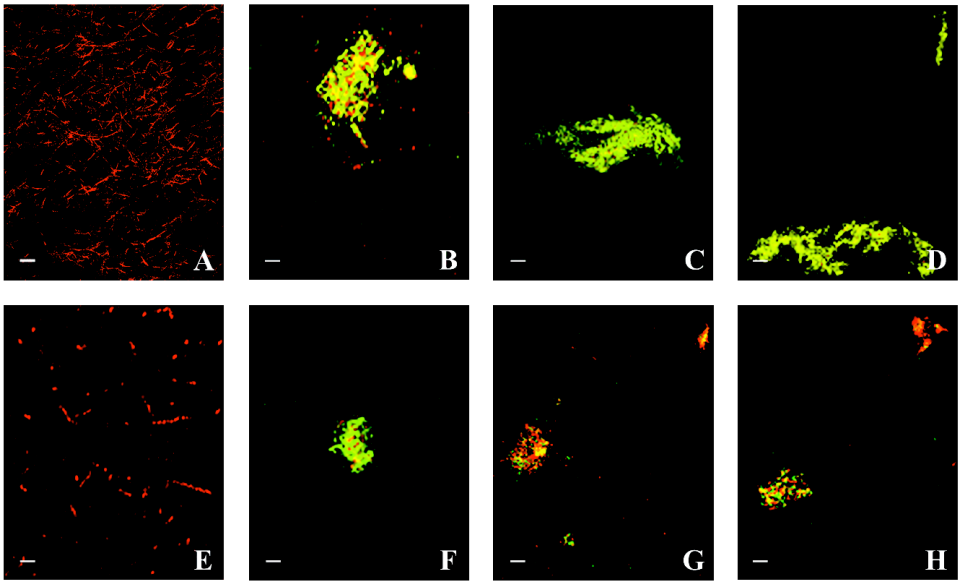

Fig. 9. Co-sedimentation assays with anti-actin immunoprecipitation pellets from GFP-FERM and GFP-FERM truncations. Magnification Bar = 5 µm. **(A)** Phalloidin-labeled muscle actin filaments prior to co-sedimentation. **(B-D)** Pellets from co-sedimentation of exogenous F-actin (red) and GFP-fusion polypeptides (green). Merged green and red fluorescence images are shown. **(B)** GFP-FERM and F-actin. **(C)** GFP-FERM-T1 and F-actin. **(D)** GFP-FERM-T2 and F-actin. **(E)** Taxol-stabilized microtubules prior to co-sedimentation. **(F-H)** Pellets from co-sedimentation of exogenous microtubules (red) and GFP-fusion polypeptides (green). Merged green and red fluorescence images are shown. **(F)** GFP-FERM and microtubules. **(G-H)** GFP-FERM, microtubules, and unlabeled muscle actin filaments.

4.15 Cosedimentation Assays of FERM With f-Actin or Microtubules

For cosedimentation essays of GFP-FERM and F-actin and microtubules, F-actin and microtubules were randomly distributed prior to use in the assay (Fig. 10A, D, G). Examination of pellets from co-sedimentation of actin filaments and GFP-fusion extracts revealed co-localization of red and green fluorescence in aggregates of actin filaments in the presence and absence of added ATP (Fig. 10B-C). In a parallel experiment, examination of pellets from co-sedimentation of microtubules and GFP fusion extracts revealed co-localization of red and green fluorescence in aggregates of microtubules (Fig. 10E-F). A control experiment used actin filaments in the presence of 10 mM Mg-ATP and an extract from cells that expressed GFP alone. Examination of the pellet from the control co-sedimentation assay did not detect co-localization of red and green fluorescence as shown in merged red and green images (Fig. 10H-I).

Fig. 10.

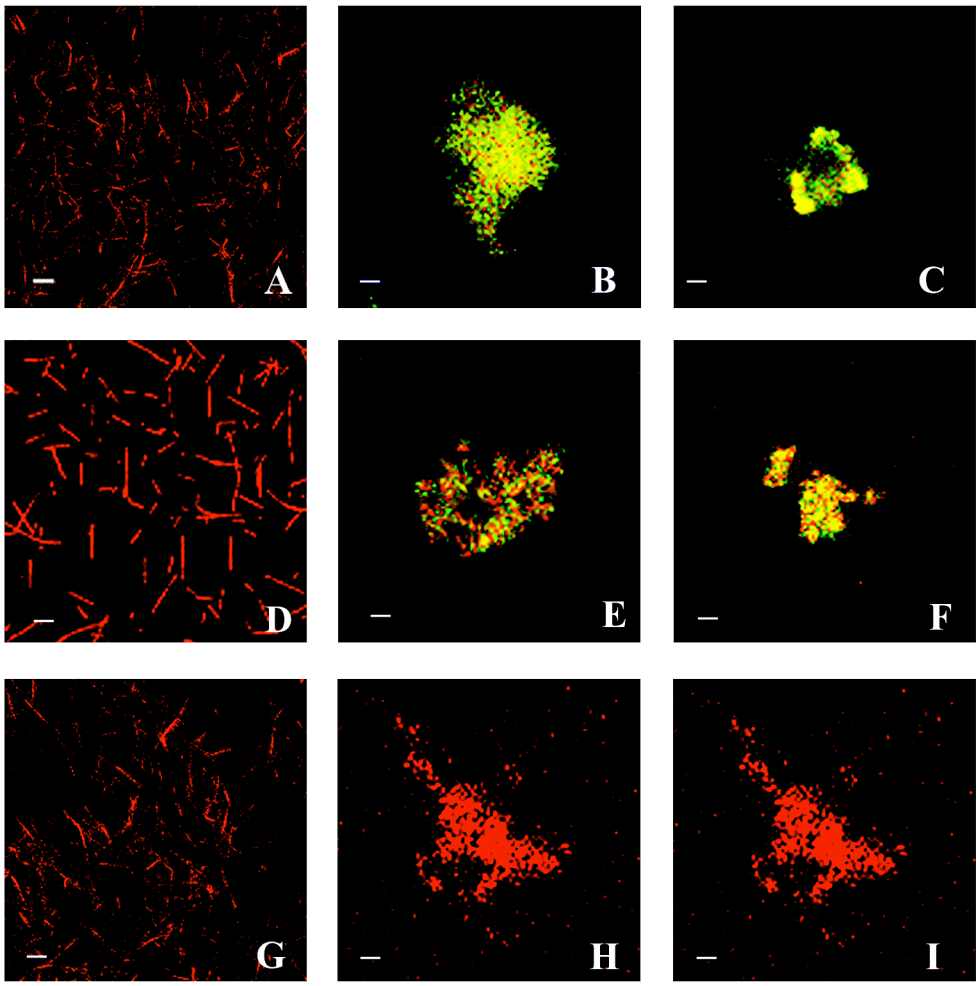

Fig 10. Cosedimentation assays with whole cell extracts of GFP-FERM overexpressing cells. Magnification Bar = 5 µm. Merged green and red fluorescence images are shown. **(A)** Phalloidin-labeled muscle actin filaments prior to co-sedimentation. **(B-C)** Pellets from co-sedimentation of exogenous F-actin (red) and extract from cells expressing GFP-FERM. **(B)** F-actin and GFP-FERM in the presence of 10 mM ATP. **(C)** F-actin and GFP-FERM in the absence of added nucleotide. **(D)** Taxol-stabilized microtubules prior to co-sedimentation. **(E-F)** Pellet from co-sedimentation of exogenous microtubules (red) and extract from cells expressing GFP-FERM. Both

images are from the same co-sedimentation pellet. **(G)** Phalloidin-labeled muscle actin filaments prior to co-sedimentation. **(H-I)** Pellet from co-sedimentation of exogenous F-actin (red) and extract (10 mM ATP added) from cells expressing GFP alone. The red channel image is shown in (H) and the merged green and red image is shown in (I).

Chapter 5 MyTH4 and FERM have distinct functions in Myo1

5.1 GFP-MyTH4 Localizes to Myo1 Targets but Predominately in the Nucleus

Cells overexpressing GFP-MyTH4 were challenged with red fluorescent beads as a marker for phagosomes and vitally stained with DAPI prior to confocal microscopy. GFP-MyTH4 localized to the macronucleus, micronucleus, phagosomes, and cytosol puncta (Fig. 11). To determine whether GFP-MyTH4 colocalizes with endogenous Myo1, overexpressing cells were challenged with blue fluorescent beads as a marker for phagosomes and immunostained with antiMyo1. Endogenous Myo1 colocalized with GFP-MyTH4 to phagosomes (Figs. 11G-11I). To further investigate colocalization of GFP MyTH4, isolated nuclei from overexpressing cells were immunostained with antiMyo1 and antiactin. In a previous report on immunolocalization of Myo1, isolated nuclei were fixed with an ethanol-triton fixative (Hosein and Gavin, 2007). In the present study, we found that paraformaldehyde fixation revealed significant localization of antiMyo1 and antiactin within the macronucleus. Both antibodies colocalized with GFP-MyTH4 to tubular or filament-like structures within the nucleus and puncta at the nuclear periphery (Figs. 11M-11K). Overexpressed GFP alone did not localize but accumulated nonspecifically in the cytosol.

Fig. 11.

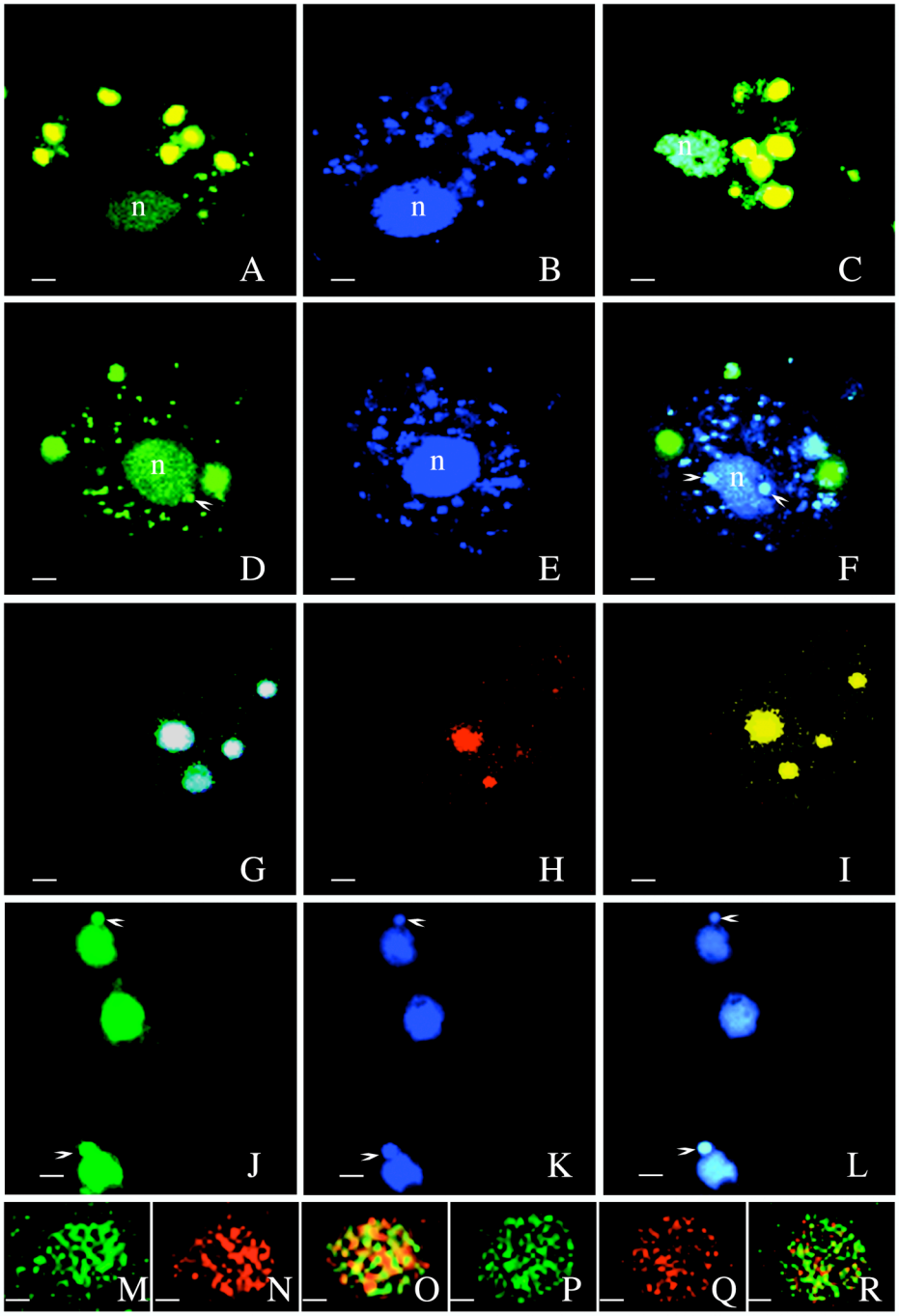

Fig. 11. Confocal images of GFP-MyTH4 localization. **(A-F)** Localization of GFP-MyTH4 in living *Tetrahymena*. Cells were stained with DAPI and imaged approximately 6 hours after initiation of GFP overexpression. Each cell was separately

imaged with green, blue, and merged green-blue channels. Macronucleus (n). Micronucleus (arrowheads). **(A-C)** Scale bar =3.7 μm. The anterior end of the cell is on the right side of each image. This cell was challenged with fluorescent beads (yellow fluorescence). **(A)** GFP signal. **(B)** DAPI signal. Numerous nuclear fragments are present in the cytosol. **(C)** Image from merged green-blue channels. **(D-F)** Scale bar =3.7 μm. This cell was not challenged with fluorescent beads. **(D)** GFP signal. **(E)** DAPI signal. Numerous nuclear fragments are present in the cytosol. **(F)** Image from merged green-blue channels. **(G-I)** Immunofluorescence localization of Myo1 in cells overexpressing GFP-MyTH4. Cells were challenged with blue fluorescent beads. Scale bar = 3.7 μm. The anterior end of the cell is at the top of each image. **(G)** Image from merged green and blue channels. **(H)** Red channel antiMyo1 signal. **(I)** Image from merged green-red channels. **(J-L)** Scale bar =6 μm. Isolated nuclei from GFP-MyTH4. Arrowheads locate the micronucleus. **(J)** GFP signal. **(K)** DAPI signal. **(L)** Image from merged green-blue channels. **(M-R)** Scale bar =xx μm. Immunofluorescence localization of Myo1 and actin in isolated nuclei from cells overexpressing GFP-MyTH4. **(M)** GFP signal. **(N)** Red channel antiMyo1 signal. **(O)** Image from merged green-red channels. **(P)** GFP signal. **(Q)** Red channel antiactin signal. **(R)** Image from merged green-red channels.

5.2 GFP-FERM Fusions Localize to Myo1 Targets but Predominately in the Cytosol

To determine whether FERM or truncations of FERM localize to Myo1 targets, cells expressing GFP-fusions were observed with confocal microscopy (Fig. 12, Table 1). Microscopy of living cells that had been challenged with fluorescent beads revealed localization of GFP-FERM to phagosomes, which often formed confluent aggregates resulting in large patches of fluorescence (Fig. 12A). GFP-FERM localized to vacuoles and puncta within nucleoplasm (Fig. 12B-C, 12D, 12F). Localization of GFP-FERM to microtubule and actin filament sites within the cytoskeleton is demonstrated by the fluorescent, crescent-shaped oral apparatus at the anterior of the cell (Fig. 12I-J), anterior to posterior fluorescent rows of basal bodies (Fig. 12I-P), and transverse fluorescent fibers between rows of basal bodies (Fig. 12N). Phagosomes and puncta associated with the anterior to posterior alignment of basal bodies (Fig. 12I-P). The puncta were often DAPI-positive (Fig. 12I-J). Localization of GFP-FERM to cilia was not observed.

Fig 12.

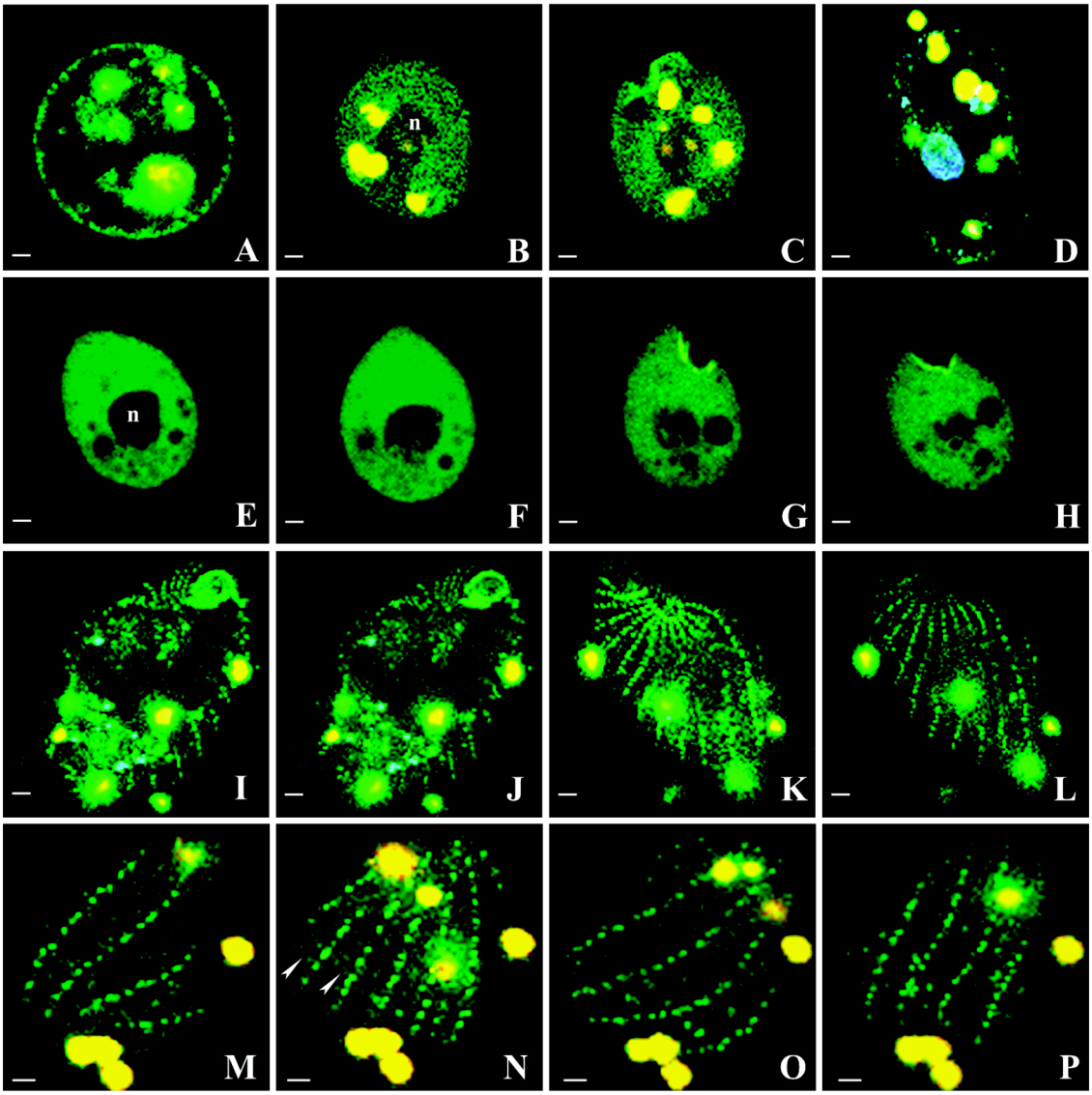

Fig. 12.

Localization of GFP-FERM in living *Tetrahymena*. Magnification Bar =3.7 µm. Fluorescent beads are yellow, n = nucleus. **(A)** A cell challenged with fluorescent beads. Cells immobilized in agarose frequently become spherical. **(B-C)** Images from a x-z series through a cell that had been challenged with fluorescent beads. Phagosomes localized to the nucleus. **(D)** A cell challenged with fluorescent beads and stained with

DAPI (blue fluorescence) to reveal the nucleus. **(E-H)** Images from a x-z series. This cell was not challenged with fluorescent beads. The intense fluorescence is from densely packed phagosomes. Vacuoles and puncta (F) localized to the nucleus. The oral apparatus (G-H) is the crescent-shaped fluorescent structure at the anterior of the cell. **(I-L)** Images from a x-z series through a cell challenged with fluorescent beads and stained with DAPI. The anterior to posterior alignment of basal bodies and the crescent-shaped oral structure (I-J) at the anterior of the cell are seen in relationship to bead-containing phagosomes. GFP-fluorescent puncta (I-J) were often DAPI-positive. **(M-P)** Images from a x-z series through a cell challenged with fluorescent beads. The cell shows the association of phagosomes with the anterior to posterior alignment of basal bodies. **(N)** GFP-FERM localized to transverse fibers (arrowheads) extending between rows of basal bodies.

5.3 GFP-MyTH4 Affects Division of the Macronucleus

Wild type *Tetrahymena* contains one macronucleus and one micronucleus. In cells overexpressing GFP-MyTH4, approximately 4% of a population was bimacronucleate, and many cells contained abundant macronuclear fragments (Figs. 5A-5C). Numerous DAPI-positive puncta accumulate at the cell surface (Fig. 5E). In some overexpressing cells, GFP-MyTH4 and DAPI colocalized to the central region of the nucleus, whereas the periphery of the nucleus did not show GFP colocalization (Figs. 5D-5F).

Fig. 13.

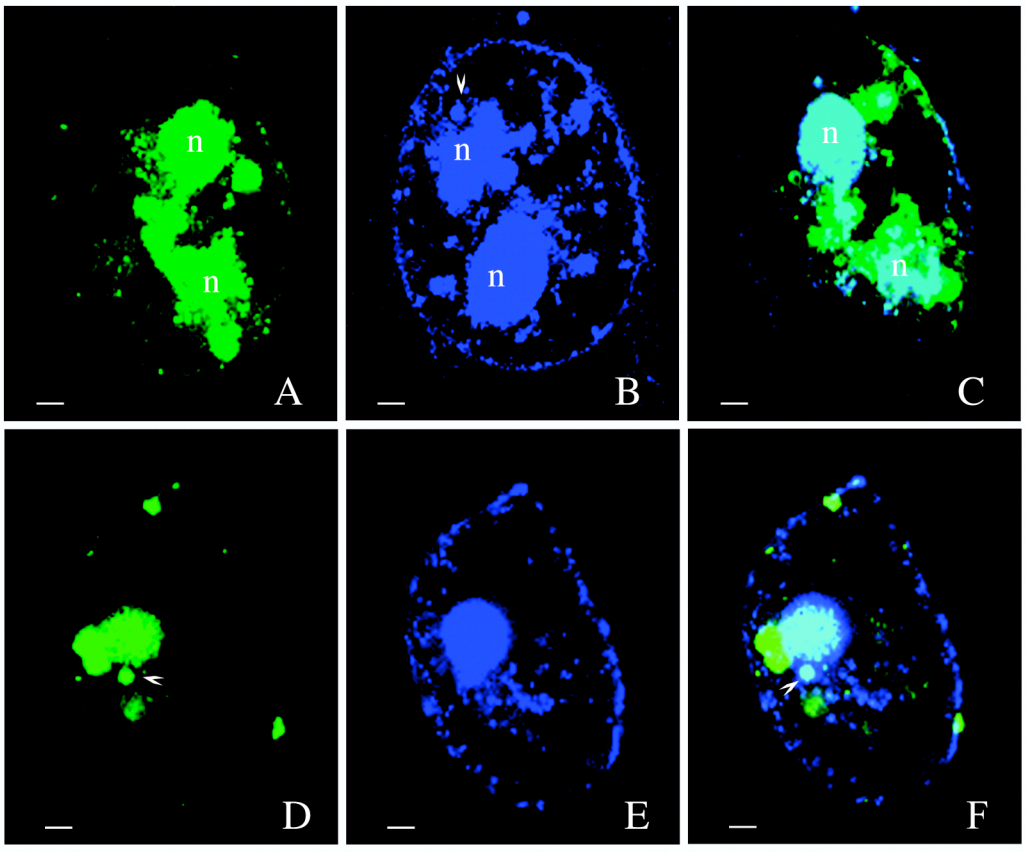

Fig. 13. Confocal images. Localization of GFP-MyTH4 in living *Tetrahymena*. Cells were stained with DAPI and imaged approximately 6 hours after initiation of GFP

overexpression. Each cell was separately imaged with green, blue, and merged green-blue channels. Macronucleus (n). Micronucleus (arrowheads). **(A-C)** Scale bar =3.7 μm. The anterior end of the cell is at the top of each image. **(A)** GFP signal. **(B)** DAPI signal. **(C)** Image from merged green-blue channels. **(D-F)** Scale bar =3.7 μm. The anterior end of the cell is at the top of each image. **(D)** GFP signal. **(E)** DAPI signal. **(F)** Image from merged green-blue channels.

5.4 GFP-MyTH4 Affects the Organization of the Intramacronuclear Microtubule Array and Elongation of the Macronucleus

Clustal alignments indicated a putative tubulin-binding site within MyTH4 (Fig. 2B). Therefore, the strong targeting of GFP-MyTH4 to the macronucleus and the occurrence of bimacronucleated cells led us to investigate the effect of overexpression on amitosis of the macronucleus with special focus on intranuclear microtubules. The organization of the intranuclear microtubules has been extensively investigated with transmission electron microscopy (Williams and Williams, 1976) and immunofluorescence microscopy (Fujiu and Numata, 2000). In amitosis, intranuclear microtubules that are initially random become oriented into an array parallel to the long axis of the cell (Fujiu and Numata, 2000; Williams and Williams, 1976). Elongation of the macronucleus is accompanied by elongation of the parallel array of intranuclear microtubules (Fujiu and Numata, 2000; Williams and Williams, 1976).

In the current study, antitubulin was used to immunostain the microtubule array and provided the basis for analyzing the effect of overexpression on the progression of microtubule elongation and nuclear elongation during amitosis (Figs. 14, 15). GFP-MyTH4 colocalized with antitubulin to intramacronuclear microtubules (Fig. 15A). A population of cells was monitored over a 12-hr period following initiation of GFP-MyTH4 overexpression. Six hours after initiation of overexpression, 80% of the cells were in stage I of amitosis in which intranuclear microtubules were assembled but not organized into a parallel array (Figs. 14, 15A, 15E). The microtubules were often thick bundles and did not appear to be affected by a 30-min exposure to nocodazole, which

depolymerized cytoplasmic microtubules (Figs. 15I-15L). Six hours after initiation of overexpression of GFP-MyTH4, only 5% of the cells had advanced to early stage II of macronuclear division in which intranuclear microtubules were partially organized into a parallel array (Figs. 14, 15M, 15Q). The orientation of the microtubule array often did not appear to be parallel to the long axis of the cell and many of the microtubules within the array did not appear to extend to the perimeter of the nucleus (Fig. 15M). Monitoring the population of overexpressing cells for an additional 6-hr period revealed that the early stage II nuclei and the parallel array of intranuclear microtubules did not achieve full elongation (Fig. 14). Constriction of partially-elongated stage II nuclei (Fig. 16M) and cytokinesis in the absence of an apparent amitosis (Fig. 15M) led to uncoupling of macronuclear division and cytokinesis. In contrast, a wild type population displayed a normal progression of amitosis over a 12-hr interval (Fig. 14). Figs. 15U-15W show an early stage in the formation of the intranuclear microtubule array in a wild type cell. In the wild type image, numerous microtubules were parallel to the long axis of the cell and extended anteriorly and posteriorly from the array to the perimeter of the nucleus. In the central region of this nucleus, the microtubules have not fully formed the parallel organization. The overexpression data for GFP-MyTH4 are consistent with the *MYO1* knockout phenotype in which the normal progression of amitosis fails to occur in some cells (Williams et al., 2000). Mitosis of the micronucleus appeared to be unaffected in the overexpression phenotype. Cell density gradually declined over a 12-hour period of overexpression.

Fig. 14.

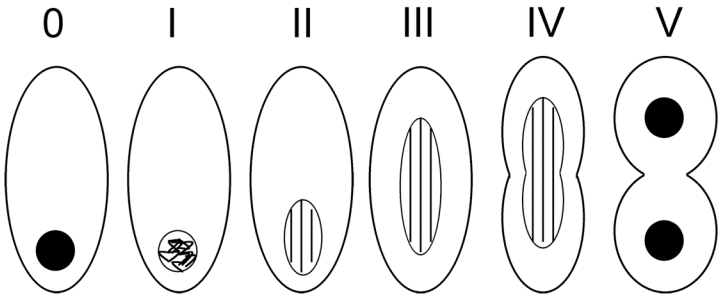

	(hrs)	(%)	(%)	(%)	(%)	(%)	(%)
MyTH4	6	15	80	5	0	0	0
WT	6	70	4	7	11	3	5
MyTH4	12	8	92	0	0	0	0
WT	12	80	5	3	6	2	4

Fig. 14. Nuclear division (amitosis) in *Tetrahymena thermophila*. Stages of amitosis (I-V) are diagrammed with emphasis on the orientation and elongation of the microtubule array and elongation of the macronucleus as observed in wild type cells immunostained with antitubulin. The distribution (%) of nuclei in various stages of amitosis is recorded for wild type and MyTH4 overexpression cells. For the overexpression phenotype, n = 320 cells analyzed. For wild type (WT) n = 210 cells analyzed. For cells expressing GFP alone (GFP) n = 88 cells analyzed. Stage 0: The interphase nucleus (dark circle). Stage I: Nucleus with random microtubules. Stage II: Elongation of the nucleus and the microtubule array. The microtubule array extends to the perimeter of the macronucleus and is parallel to the long axis of the cell. Stage III: Intranuclear microtubules elongate. Cytoplasmic microtubules that connect the nuclear envelope with the cell periphery are not shown. Stage IV: Constriction of the

macronucleus at its midpoint. Stage V: Completion of macronuclear separation. Diagram redrawn from Williams et al. (2000).

Fig. 15.

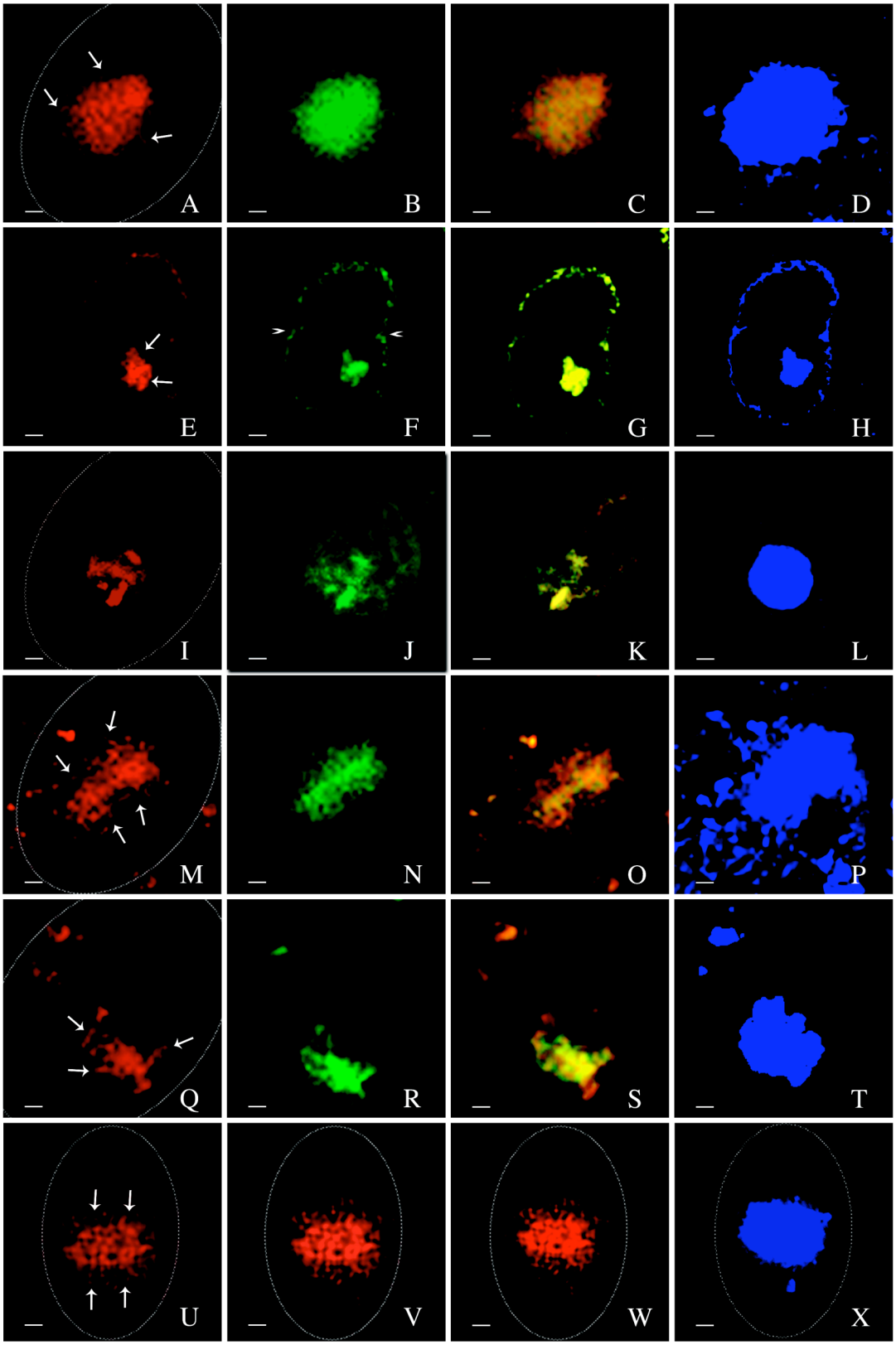

Fig. 15. Immunofluorescence localization of tubulin in GFP-MyTH4 overexpressing cells. Cells were fixed 6-hrs after induction of GFP expression. Each cell was separately imaged with green, red, and blue channels and with merged green-red channels. The anterior end of the cell is at the top of each image. The white lines allow identification of the long axis of the cell. However, in each image the cell is magnified larger than the boundary indicated by the white lines. **(A-T)** Cells expressing GFP-MyTH4. **(A-D)** Scale bar =1.5 µm. Macronucleus in Stage I of nuclear division. **(A)** Antitubulin signal. Intramacronuclear microtubules are evident throughout the nucleus. Representative microtubules are identified by arrows. Tubulin localization to the cortex is not evident in this optical section. **(B)** GFP signal. **(C)** Image from merged green-red channels. GFP-MyTH4 and antitubulin show significant colocalization. **(D**) DAPI signal. **(E-H)** Scale bar =5.5 µm. Macronucleus is in stage I. A division furrow (arrowheads) has formed and cytokinesis will produce an amacronucleate subcell. **(E)** Antitubulin signal. Microtubules appear as thick bundles (arrows). **(F)** GFP signal. **(G)** Image from merged green-red channels. **(H)** DAPI signal. Numerous DAPI-positive puncta accumulate at the cell surface. **(I-L)** Scale bar =3.7 µm. Macronucleus in stage 1 in a cell treated with nocodazole. **(I)**. Antitubulin signal Microtubules appear as thick bundles. **(J)** GFP signal. **(K)** Image from merged green-red channels. **(L)** DAPI signal. **(M-P)** Scale bar =1.5 µm. Macronucleus in stage II of nuclear division. **(M)** Antitubulin signal. Representative microtubules within the intramacronuclear microtubule array are identified by arrows. **(N)** GFP signal. **(O)** Image from merged green-red channels. GFP-MyTH4 and antitubulin show significant colocalization. **(P)** DAPI signal. Macronuclear fragments are abundant throughout the cytosol. **(Q-T)** Scale bar =1.5 µm.

Macronucleus is in stage II. **(Q)** Antitubulin signal. Representative microtubules within the intramacronuclear microtubule array are identified by arrows. **(R)** GFP signal. **(S)** Image from merged green-red channels. **(T)** DAPI signal. **(U-X)** Scale bar =1.5 μm. Optical sections through an early stage II macronucleus in a wild type cell. **(U-W)** Antitubulin signal. **(X)** DAPI signal.

5.5 Overexpression of a Truncated MyTH4

To determine whether deletion of the putative tubulin binding site within MyTH4 affected the association of MyTH4 with tubulin, a truncated MyTH4 domain that eliminated the putative tubulin binding motif was fused with a GFP construct and used to transform *Tetrahymena*. However, this construct induced death upon induction, and data was not able to be collected.

5.6 GFP-FERM Affects the Trafficking of Phagosomes and Membrane Recycling at the Cytoproct

In *Tetrahymena*, phagosomes are formed in the feeding structure known as the oral apparatus at the anterior portion of the cell. They are processed into digestive feeding structures by fusion with lysosomes while transported to the posterior region of the cell. The membrane material is recycled in the posterior region of the cell by an organelle known as the cytoproct. The distribution of fluorescence from GFP-FERM is consistent with localization to the basal body-associated filament complex and transverse microtubule bands (Fig. 12N). In the overexpression of GFP-FERM truncations, phagosomes accumulate at the posterior region of the cell (Fig 16) and it seems that this caused by the overexpression of GFP-FERM truncations. Localization of MyTH4 (Fig. 11), truncated FERM domains containing either the FERM N-terminus region (Fig. 16A-D) or the FERM C-terminus region (Fig. 16E-H) was strikingly different from the localization of GFP-FERM (Table 1, Fig. 12). GFP-MyTH4 localizes to the nucleus. Truncated FERM domains localized to phagosomes but not to the cytoskeleton or the nucleus. Confluent aggregates of phagosomes were often located in the posterior region

of cells over-expressing truncated FERM domains. Cells expressing GFP without FERM displayed un-localized fluorescence throughout the cytosol.

Fig 16.

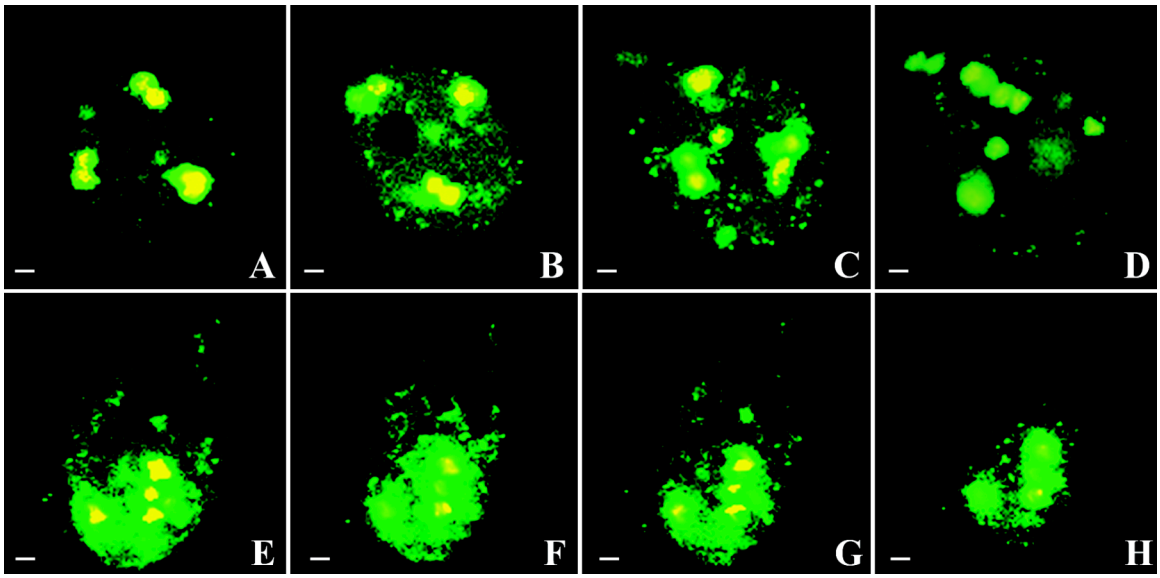

Fig 16. Localization of truncated GFP-FERM domains in living *Tetrahymena* challenged with fluorescent beads (yellow). Magnification Bar =3.7 μm. **(A-D)** Localization of GFP-FERM-T1 containing the N-terminal region of FERM. Images from a x-z series. **(E-H)** Localization of GFP-FERM-T2 containing the C-terminal region of FERM. Images from a x-z series.

Chapter 6 Discussion for MyTH4 and FERM

6.1 Overexpression of GFP Fusions

Expression of *Tetrahymena* genes in heterologous hosts such as bacteria is highly problematic due to the unusual codon usage in *Tetrahymena* (Horowitz and Gorovsky, 1985) in which TAA and TAG code for glutamine. Myo1 MyTH4 contains 7 and FERM contains 49 TAA or TAG stop codon triplets. Therefore, in this study, the *Tetrahymena* expression system is the method of choice for investigating interactions between MyTH4 and FERM and cytoskeleton proteins. Homologous-host expression allows investigation of endogenous binding partners whether direct or indirect.

6.2 MyTH4 Interacts With Intranuclear Tubulin and Actin

Antiactin coprecipitates GFP-MyTH4, tubulin, actin, and Myo1. AntiGFP affinity pulls down GFP-MyTH4, tubulin, and actin. These two experimental observations are strong indications that GFP-MyTH4 interacts with tubulin and actin. However, presence of additional proteins in both the IP and the antiGFP pulldown makes it difficult to conclude whether the binding of actin and tubulin is direct or indirect. In the cosedimentation experiments, MyTH4 associates with crosslinked F-actin and crosslinked microtubules. If there were direct binding of tubulin and actin to MyTH4, crosslinking of the polymers could be problematic because Clustal W alignments suggest only a single putative tubulin binding site and one actin binding site within MyTH4. Therefore, if the observed crosslinking were a function of direct binding to MyTH4, interaction between two MyTH4 domains would be required. Studies of FERM-FERM interactions indicate MyTH4-MyTH4 interactions are at least feasible. ERM family proteins, e.g., ezrin are known to exist as monomers and dimers, and two associated

FERM/ C-ERMADs (C-terminal ERM association domain) have been proposed to exist within the dimer (Chambers and Bretscher, 2005; Bretscher et al., 1995). Studies of radixin FERM dimers identify a sequence that is proposed as the site involved in dimerization of FERM (Kitano et al. 2006). Interestingly, the radixin sequence loosely matches a sequence in Myo1 FERM (Gotesman et al., 2010) and in Myo1 MyTH4 (Fig. 2). In the light of these studies of ERM proteins, it is therefore intriguing to speculate that for Myo1 both FERM and MyTH4 could form dimers. Formation of MyTH4 dimers or dimerization of MyTH4 with any of the five *Tetrahymena* myosins that contain MyTH4 domains could be sufficient for crosslinking either microtubules or F-actin. Crosslinking of F-actin occurs in the presence and absence of added nucleotide and is therefore independent of the actin-binding site in the myosin motor domain.

6.3 MyTH4 Localizes to Myo1 Targets and Affects Myo1 Function

Two important observations indicate MyTH4 targets the same sites as Myo1 and affects Myo1 function. GFP-MyTH4 and Myo1 colocalize to the interior to the nucleus, and the GFP-MyTH4 overexpression phenotype partially mimics the *MYO1* knockout phenotype. In both overexpressing cells and *MYO1*-knockout cells, macronuclear elongation fails to properly occur, cytokinesis and division of the macronucleus are uncoupled, and consequently, division progeny often contain two macronuclei or no macronucleus.

6.4 Elongation and Constriction of the Macronucleus

The precise role of intranuclear microtubules in elongation and constriction of the nucleus is not fully understood. It is unclear whether polymerization of microtubules or sliding of microtubules is a driving force for nuclear elongation. Alternatively,

elongation of microtubules could depend upon elongation of the nucleus. Two studies specifically connect tubulin with effects on nuclear elongation and constriction. In one study, a mutation in a beta tubulin gene is associated with failure of macronuclear elongation and constriction resulting in amacronucleated cells at cytokinesis (Smith et al., 2004). Another study suggests that force production for elongation and constriction does not depend entirely on microtubule dynamics. Macronuclei in colchicine-treated cells initiate the elongation process in the absence of intranuclear microtubules, but the nuclei do not fully elongate and do not constrict into two subnuclei (Williams and Williams, 1976). Application of colchicine to fully elongated macronuclei does not prevent constriction into subnuclei.

Elongation and constriction of the macronucleus could also involve actin, perhaps in association with microtubules. Antibodies against actin and Myo1p colocalize to the the macronucleus. Knockout of *MYO1* severely impairs elongation of the nucleus during nuclear division and is indirect evidence that actin is involved in elongation (Williams et al., 2000). Interestingly, knockout of an actin gene (*ACT1*) in *Tetrahymena* does not appear to affect cytokinesis or nuclear division (Williams et al., 2006). However, overexpression of *ACT1* leads to failure of macronuclear elongation (Hosein et al., 2003).

6.5 Overexpression of GFP-MyTH4 Affects Organization of the MT Array, a Possible Driving Force for Elongation of the Macronucleus

During a 12-hr period of overexpression of GFP-MyTH4, more than 90% of the cells are permanently arrested in stage I of amitosis, and the intranuclear microtubules fail to become organized into a parallel array. The microtubules appear as thick bundles suggesting a highly crosslinked structure. Interestingly, nocodazole did not appear to

affect the bundle-like appearance of intranuclear microtubules, perhaps due to extensive crosslinking of the microtubules. Five percent of overexpressing cells organize the intranuclear microtubules into a parallel array, but the microtubules and nucleus fail to achieve full elongation. Partially-elongated nuclei apparently constrict into two subnuclei that remain in one subcell at cytokinesis thereby producing bimacronucleate and amacronucleate subcells and uncoupling nuclear division and cytokinesis (Fig. 13G-13I). Additionally, overexpression appears to lead to an aberrant orientation of the microtubule array, which is not parallel to the long axis of the cell (Fig. 14E). Failure of intramacronuclear microtubules to form parallel arrays, failure of the macronucleus to elongate, and aberrant constriction of the macronucleus indicate MyTH4 interaction with microtubules affects microtubule organization and elongation of the macronucleus. One could argue that elongation of the macronucleus requires a parallel array of microtubules and that polymerization of microtubules within the array could be a driving force for nuclear elongation.

6.6 GFP-MyTH4 Affects Myo1 Function

Several observations suggest that GFP-MyTH4 specifically contributes to Myo1 function and that it is unlikely the GFP-MyTH4 phenotype is a nonspecific effect of overexpressed GFP. GFP-MyTH4 and Myo1 colocalize, and the overexpression phenotype mimics the knockout phenotype with respect to elongation of the macronucleus and uncoupling of macronuclear division and cytokinesis. GFP-MyTH4 specifically targets intramacronuclear microtubules and is not randomly accumulated in the nucleus. Targeting of GFP-MyTH4 to intranuclear microtubules could involve a specific posttranslational modification of these microtubules (Gaertig and Wloga, 2008;

Hammonda et al., 2008; Wloga et al., 2008). Furthermore, overexpression of other GFP-tagged, truncated tail domains does not lead to accumulation of GFP in the nucleus. For example, overexpressed truncated GFP-FERM domains comparable in molecular mass to GFP-MyTH4, do not localize to the nucleus (Gotesman et al., 2010). Interestingly, GFP-tagged MyTH4 from Myo9 (amino acids 1049 through 1226), another *Tetrahymena* myosin, does not localize and is distributed diffusely throughout the cytosol (unpublished data). We argue that in light of these various observations, overexpresssed MyTH4 contributes to Myo1 function.

6.7 Proposed Model for Interaction Between MyTH4 and Microtubules

A proposed model for interaction between MyTH4 and microtubules is shown in Fig. 17. The model is based on a proposed dimerization of MyTH4 in a manner suggested by the reported dimerization of FERM (Kitano et al., 2008) and is consistent with either polymerization of microtubules or sliding of microtubules as the driving force for elongation of the macronucleus. MyTH4 is proposed to bind to the plus end of microtubules and proposed MyTH4 dimers could crosslink microtubules, converting random microtubules into an array that is oriented parallel to the long axis of the cell. In overexpressing cells, the orientation of the microtubule array frequently is not parallel to the long axis of the cell. Overabundance of MyTH4 could lead to excessively crosslinked microtubules, which would not form parallel arrays. Another prediction of the model is that overabundance of MyTH4 accumulates at the plus ends of microtubules and could create a cap that could prevent elongation of microtubules and thereby eliminate the force of polymerization required for elongation of the nucleus. Cosedimentation assays are consistent with the proposed model. GFP-MyTH4

cosediments with crosslinked microtubules in which MyTH4 appears to be localized at one end a microtubule (Fig. 7L, Inset). Colocalization of GFP-MyTH4 and antitubulin is also consistent with the proposed model. The central region of the microtubule array displays the most prominent colocalization of GFP-MyTH4 and antitubulin. Microtubules extend from this region of intense colocalization (Figs. 15G, 15K). The proposed model, at best, could account for only part of the machinery required for elongation of the nucleus. Studies of microtubule inhibitory drugs indicate that force production for elongation of the nucleus does not depend entirely on microtubule dynamics (Williams and Williams, 1976).

Fig. 17.

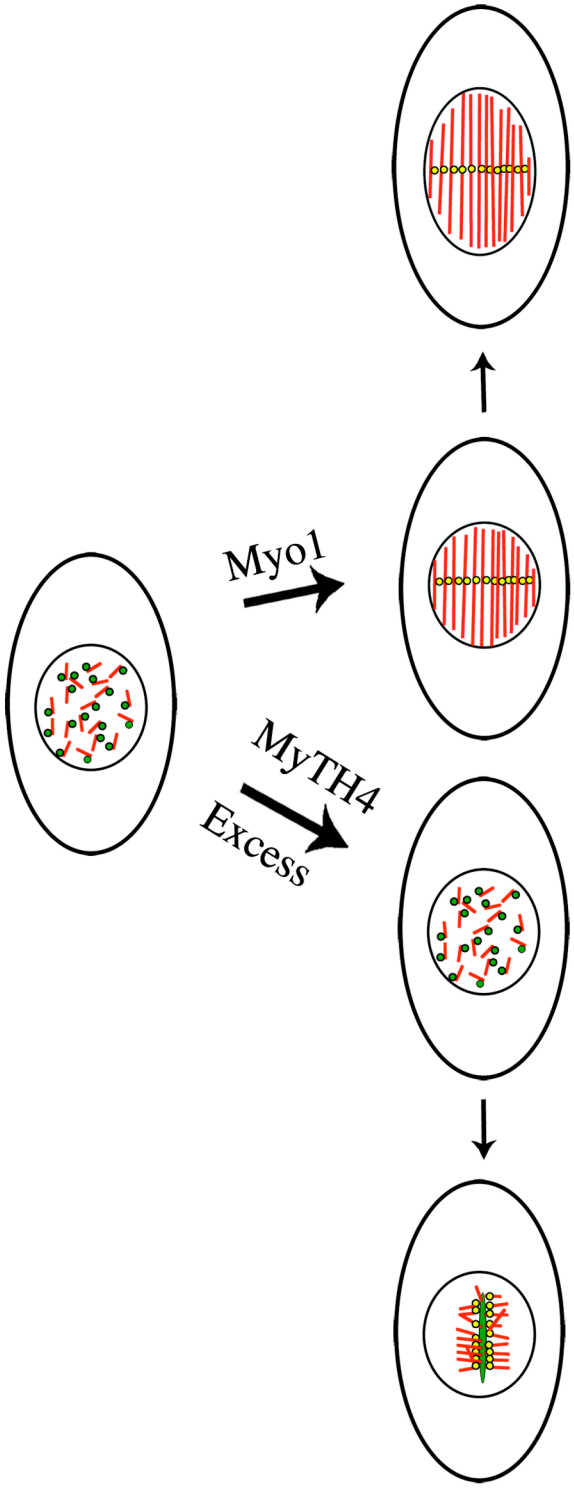

Fig. 17. A proposed model for the role of MyTH4 in the organization of a microtubule array. Green = MyTH4, Red = crosslinked microtubules, Yellow = Overlap between MyTH4 and microtubules. Myo1p through its MyTH4 domain is proposed to bind to the plus end of microtubules and crosslink the microtubules, which form an array oriented parallel to the long axis of the cell. Elongation of the microtubule array is accompanied by elongation of the nucleus as shown at the top of Fig. 16. Excess (overexpression) of MyTH4 is proposed to create a cap at the microtubule plus end, and consequently, the microtubules do not reach the perimeter of the nucleus and the orientation of the array often appears aberrant (Image at bottom of Fig. 15).

6.8 Analysis of GFP-FERM Overexpression in Tetrahymena thermophila

Immunoblot analysis confirms the predicted molecular mass for the GFP-fusion polypeptides (Fig. 7). Some fusion polypeptides from strain GFP-FERM-T2 are higher in molecular mass than the predicted value, a probable indication of post-translational modification. The three transformed strains that overexpress FERM or a truncated FERM have apparently different physiological states as indicated by the large variation in generation times and the significant cell death in the strains expressing a truncated FERM. The three strains could have perturbations in actin and tubulin dynamics. Variations in gel profiles of IP pellets from the three strains most likely reflect the apparent physiological state of each strain.

6.9 Myo1 FERM interacts with actin filaments and microtubules.

Immunoprecipitation assays indicate Myo1 FERM interacts with actin and tubulin. Actin antibody co-immunoprecipitates GFP-fusions and tubulin from lysate of strains that over-express GFP-fusions (Fig. 7C-D). Actin antibody immunoprecipitates tubulin but not GFP from lysate of the strain expressing GFP alone (Fig. 7C-D). Therefore, it appears unlikely that GFP interacts non-specifically with proteins in IP pellets.

Co-sedimentation assays reveal that fluorescence from either actin filaments or microtubules co-localizes with GFP fluorescence in whole cell extracts (Fig. 9) and IP pellets (Fig. 10) from strains expressing GFP-fusions but not in cell extract from the strain expressing GFP alone (Fig. 7). These two co-sedimentation assays provide strong evidence that Myo1 FERM interacts with both actin and tubulin and that the interactions are not attributable to non-specific binding of GFP. Interactions with actin and tubulin

could be achieved through direct binding with FERM or through indirect binding involving accessory proteins that are associated with FERM. SDS-PAGE analysis reveals several polypeptides in the anti-actin immunoprecipitation pellets consistent with numerous actin-binding and tubulin-binding proteins that are potential sites for indirect binding of actin and tubulin to FERM (Fig. 7B). The two putative actin-binding and tubulin-binding sequences in FERM could cross-link and stabilize actin filaments and microtubules, respectively. Each truncated GFP-FERM domain contains only one actin-binding sequence and one tubulin binding sequence. However, each truncated FERM contains a sequence motif for possible dimerization of FERM in vivo and in vitro. Endogenous Myo1 and other FERM-containing myosins could dimerize with over-expressed FERM and contribute to cross-linking activity. Addition of actin filaments to microtubule co-sedimentation assays does not appear to significantly enhance the aggregation of microtubules, an indication that FERM does not appear to influence direct interactions between actin filaments and microtubules.

Existence of ERM-like binding motifs in the FERM domain and other regions of Myo1 indicate this myosin could have functions that are independent of its actin-dependent ATPase activity. ERM-family proteins are inactive when intramolecular binding of FERM to the C-ERMAD masks binding sites within FERM (Pearson et al., 2000). Kitano et al. (2006) point out that in both ezrin and radixin, the KxxTIxVxxM motif overlaps with the actin-binding site and suggest that the motif is involved in regulation of actin binding. One or both of the KxxTIxVxxM sequences in Myo1 FERM could be masking motifs that regulate accessibility of actin-and tubulin-binding sites. Interestingly, the KxxTIxVxxM motif in the C-terminal region of Myo1 FERM overlaps

with both the C-terminal actin-binding sequence and the C-terminal tubulin-binding sequence. Another potential function of the KxxTIxVxxM motif could be intermolecular binding of FERM to form a Myo1 dimer in the absence of apparent coiled-coil domains in the Myo1 tail. Dimerization of Myo1 could facilitate its motor activity on actin filaments. A putative FERM binding motif (TKQRIDEFEAL) in the Myo1 motor domain could provide a site for interaction between FERM and the motor and effectively mask a binding site for a ligand that, in some way, is involved in regulation of motor activity. Binding of FERM to the motor would require a conformational change such that the Myo1 tail would be bent against the motor. Interestingly, studies of a class VII myosin reveal that in an ATP-dependent manner, the tail domain is bent against the motor domain and that deletion of a sub-domain within FERM eliminates bending (Yang et al., 2009).

6.10 FERM is Involved in Localization of Myo1

Previous investigations of Myo1 and actin utilized over-expression of GFP-actin and immunostaining with a peptide antibody that detects the full-length Myo1 (Hosein et al., 2003, 2005; Hosein and Gavin, 2007). GFP-actin localizes to the cytoskeleton and phagosomes. The Myo1 peptide antibody localizes to phagosomes, vacuoles, and puncta within nucleoplasm, and weakly immunostains basal bodies within the cytoskeleton as evident in the peripheral immunolabeling of the cell in Fig. 2j and 2l of Hosein and Gavin (2007). In the present study GFP-FERM localizes to the cytoskeleton, phagosomes, and both cytoplasmic and nuclear puncta (Fig. 12). The punctate localization of Myo1 FERM to the nucleus is consistent with the apparent punctate nuclear localization of another class XIV myosin, *Pfmyo-D* in *Plasmodium falciparum* (Chaparro-Olaya et al., 2005).

GFP-labeled puncta in the cytosol were frequently DAPI-positive and therefore could be extruded chromatin from the macronucleus. Wild type *Tetrahymena* frequently eliminates chromatin from the macronucleus (Cleffmann, 1980). Even though the GFP-FERM construct eliminates all of the Myo1 sequence N-terminus of FERM, the truncated tail localizes to the same targets as the full length Myo1. This finding is a strong indication that FERM is significantly involved in localization of Myo1 to all of its known targets.

Localization of GFP-FERM to puncta and vacuoles within the nucleus indicates trafficking of vacuoles to the nucleus as previously reported (Hosein and Gavin, 2007). This highly unusual trafficking to the nucleus could involve a NLS associated with the vacuole membrane. NLS-like sequences are revealed in an alignment of Myo1 FERM with the NLS (PPKKKRKVED) for Simian virus 40 large T antigen, and a recent study (Rahaman et al., 2008) demonstrates that the SV40 NLS can target proteins to the nucleus in *Tetrahymena*. Localization of FERM to the nucleus is consistent with presence of NLS-like sequences in both the N-terminus and C-terminus regions of FERM. Failure to observe localization of truncated FERM domains to the nucleus is an indication that nuclear localization of FERM requires interaction between N-terminus and C-terminus sequences within FERM. How vacuoles interact with the nuclear envelope is unknown, but at least one experimental model involving liposomes should be noted. ERM family proteins can induce reversible holes in liposomal membranes assembled from neutral and acidic phospholipids (Saitoh et al., 1998; Takeda et al., 2006). Talin-induced holes in giant liposomes can allow entry of a spherical liposome larger than 1.0 μm (Saitoh et al., 1998; Takeda et al., 2006). Although it seems unlikely that perforation of cellular

membranes occurs in vivo, the liposome model at least raises the possibility that ERM family and ERM-like proteins function in reversible reorganization of membrane structure that could drastically alter traffic across the membrane.

Microtubules and actin filaments could mediate localization of FERM. GFP-FERM localizes to basal bodies but apparently not to cilia, and it is intriguing to suggest the possibility that FERM interacts with a post-translational modification such as tubulin glutamylation, which involves two enzymes that could modify different sites on tubulin in basal bodies and cilia (Gaertig and Wloga, 2008; Hammonda et al., 2008; Wloga et al., 2008). Truncated FERM domains contain either the N-terminus region or C-terminus region of FERM and only one tubulin-binding sequence and one actin-binding sequence. The truncated domains fail to localize to the nucleus and basal bodies (Fig. 13), possibly a reflection of reduced ability to interact with microtubules and actin filaments. Although localization of FERM can apparently occur independent of other regions of Myo1, it is possible that redundancy of function within the tail domain could provide multiple regions that affect localization of Myo1 independent of its FERM domain. That either the N-terminus region or the C-terminus region of FERM localizes to phagosomes indicates redundancy of function within the Myo1 tail domain.

6.11 Phagosome Motility on Cortical Rows of Basal Bodies?

Phagosomes align along the anterior to posterior axis of *Tetrahymena* and move toward the posterior of the cell while maintaining the alignment (Hosein et al., 2005). In *MYO1* knockout, phagosomes are much less likely to be aligned, and their movement is random rather than directed toward the posterior of the cell (Hosein et al., 2005). Putative interaction of phagosomes with basal bodies and the directed nature of

phagosome motility could depend on transient attachments between phagosomes and basal body-associated structures within the cell cortex. Cortical structures that could provide transient attachment sites for vacuoles include the actin-rich filament complex surrounding each basal body (Hoey and Gavin, 1992) and transverse microtubule bands extending between rows of basal bodies (Allen, 1967). The distribution of fluorescence from GFP-FERM is consistent with localization to the basal body-associated filament complex and transverse microtubule bands (Fig. 12N).

6.12 MyTH4 and FERM Have Overlapping and Distinct Roles in Myo1 Function

Coimmunoprecipitation, antibody pulldown, and cosedimentation assays indicate both MyTH4 and FERM interact with tubulin and actin (directly or indirectly), and therefore the two domains display overlapping functions. Localization of MyTH4 and FERM is consistent with distinct functions for the two domains in Myo1p. MyTH4, independent of FERM strongly targets intranuclear microtubules, whereas FERM, independent of MyTH4, localizes to the cytoskeleton. Overexpressed N-terminus and C-terminus truncated FERM domains do not localize to the cytoskeleton (Gotesman et al., 2010). Therefore, the entire FERM domain, independent of MyTH4, is a sufficient and required domain for localization to the cytoskeleton.

The contrast between phenotypes from overexpression of either MyTH4 or FERM is a further indication of distinct roles for the two domains. Overexpression of GFP-MyTH4 adversely affects organization and elongation of intramacronuclear microtubules, elongation of the macronucleus, and the coupling of nuclear and cytoplasmic division. Trafficking of phagosomes does not appear to be affected in the GFP-MyTH4 phenotype.

The GFP-MyTH4 overexpression phenotype is severe and over time becomes lethal, a likely consequence of overabundance of MyTH4 bound to targets of wild type Myo1. In contrast to overexpression of GFP-MyTH4, cells overexpressing GFP-FERM do not appear to have abnormalities in elongation and constriction of macronuclei, but phagosomes abnormally accumulate at the membrane recycling site in the posterior end of cells overexpressing a C-terminus truncated FERM domain (Gotesman et al., 2010).

A summary of the distinct localization and roles for MyTH4 and FERM is shown in table 1.

TABLE 1. Localization of Myo1 MyTH4 and FERM

Domain	Construct	Localization
MyTH4	(GFP-MyTH4)	intranuclear microtubules, phagosomes
N-terminus MyTH4	(GFP-MyTH4T)	expression is lethal
FERM	(GFP-FERM)	phagosomes, cytoskeleton, nucleus
N-terminus FERM	(GFP-FERM-T1)	phagosomes
C-terminus FERM	(GFP-FERM-T2)	phagosomes

Table 1. Localization of Myo1 MyTH4 and FERM

Chapter 7 Concluding Summary

Five of the thirteen Tetrahymena thermophila myosins consist of a MyTH4/FERM domain that is common to human class VII, X, XV myosins, nematode class XII myosin, and the divergent *Dictyostelium* myosin, MyoG. The role of the MyTH4/FERM domains in the function of these myosins is poorly understood. This dissertation separates MyTH4 and FERM into separate domains to determine how each domain serves to function Myo1. We examined whether these domains have similar, overlapping or discrete roles in the function of Myo1.

Biochemical evidence shows MyTH4 and FERM, to be similar. Each domain is pulled down by lowspeed centrifugation by exogenous f-actin or microtubules; implying that these domains act in a complex that crosslinks f-actin and microtubules, and possibly to each other. Both domains are found in fractions that were separately co-immunoprecipitated with antiactin. Those fractions were also enriched with tubulin. And those co-immunoprecipitated fractions that are enriched with GFP-Myo1 tail truncations retained both f-actin and microtubular crosslinking abilities.

However, confocal Microscopy of GFP-MyTH4, GFP-FERM, and GFP-FERM truncations revealed that each domain localizes in a distinct pattern of Myo1 targets. GFP-MyTH4 localizes predominately to the nucleus, and colocalizes to intranuclear microtubules in conjunction to localizing to phagosomes. Whereas, GFP-FERM localizes to phagosomes, and sparsely to the nucleus as puncta. And GFP-FERM truncations localize to phagosomes and the cytoskeleton. Phenotypic analysis of overexpression of distinct GFP-Myo1 truncations reveals that GFP-MyTH4 disrupts the transition from stage I to Stage II during amitosis in *Tetrahymena*, by affecting the crosslinking pattern

of intranuclear microtubules. Whereas, overexpression of FERM affects phagosome trafficking and recycling at the cytoproct.

Complete localization of FERM to Myo1 targets is consistent with a parallel study in which a Class VII Myosin (Myo7A) truncated for the second FERM domain in mice fails to localize to melanosomes, leading to hair bundle defects (Shwander et al., 2009). Also, MyoVIIa knockout in *Dictyostelium discodium* inhibits phagocytosis, possibly by disrupting phagosome trafficking (Titus, 1999; Tuxworth et al, 2001). Similarly, phagocytosis is affected in bovine pulmonary alveolar macrophages (PAMs) by inhibition of Myo10, a MyTH4/FERM myosin and expression of Myo10-headless truncations (Cox et a., 2002). Therefore, the role of Myo1-FERM in affecting phagosome recycling, localizing to myo1 targets, and interacting with f-actin is consistent with current research in other FERM myosins. However Myo1-FERM interacting with microtubules is a novel finding of this work.

Myo1 in *Tetrahymena thermophila* may associate with microtubules by the MyTH4/FERM region or by a novel region demonstrated by the ability of MyoVa (a non-MyTH4/FERM myosin) to "randomly diffuse back and forth" on microtubule tracks (Ali et al., 2006). During nuclear division of *Lecudina tuzetae*, the nuclear envelope does not breakdown, microtubule polymerization may act as the "pushing force" to separate the dividing nucei in *L. tuzetae* (Kuriyama et al., 2005). If a similar process takes place in *Tetrahymena*, then overexpression of the GFP-MyTH4 can crosslink nuclear microtubules and thereby arrest nuclear division. The six *Plasmodium falciparum* class XIV myosins, PfmyoA-F, are differentially expressed in during malaria development and PFmyoD localizes to segregating nuclear material during the schizont phase of

development (Chaparro-Olaya et al, 2005). Accordingly, another class XIV myosin, Myo1, localizes to the nucleus and affects intranuclear microtubules during macronuclear elongation and is maximally expressed during conjugation.

It appears that MyTH4 and FERM domains have similar and overlapping roles in the function of Myo1. MyTH4 and FERM function in the crosslinking of f-actin, microtubules, and possibly the crosslinking of f-actin to microtubules. However, MyTH4 and FERM are active in different regions of *Tetrahymena*. MyTH4 functions in the nucleus during the elongation of intranuclear microtubules at macronuclear division, whereas FERM functions in the cytosolic regions of the cell, at the cytoskeleton and phagosome and is involved in trafficking phagsomes from the oral apparatus to the cytoproct and in recycling of membrane material at the cytoproct. Therefore, MyTH4 and FERM have overlapping roles in the function of Myo1 in terms of association with actin and tubulin. However, MyTH4 localizes and functions in the nucleus and FERM localizes and functions in the cytosol and therefore, MyTH4 and FERM have distinct responsibilities in Myo1 function. Although many roles for myosin in the nucleus have been reported, the exact function of Myo1 in the *Tetrahymena* nucleus is unclear. But our speculation that Myo1 is involved in orienting intranuclear microtubules during macronuclear elongation is consistent with findings that the MyTH4 region of Myo10 in *Xenopous oocytes* orients spindle pole bodies during mitosis (Sandquist et al., 2009; Sandquist and Bement, 2010). The results could provide new insight into the function of MyTH4 and FERM domains in myosins, kinesins, and non-motor proteins.

Chapter 8 Methods

Materials and Methods:

Creation of Overexpression Constructs

All MYO1 and Myo1 sequences were accessed using accession code U87268.2 from the National Center for Biotechnology Information (http://www.ncbi.nlm.nih.gov/). The physical characteristics were analyzed using the protparam tool at The ExPASy (Expert Protein Analysis System) proteomics server of the Swiss Institute of Bioinformatics (SIB) (http://www.expasy.ch/tools/protparam.html). Conserved domain database (CDD) (Marchler-Bauer and Bryant 2004; Marchler-Bauer A et al. 2005; Marchler-Bauer and et al. 2007), and Prosite (Hulo and et al., 2007) was used to model the updated sequence of Myo1. ClustalW (Kyoto University Bioinformatics Centers) alignment of the Myo1 sequence with calmodulin-binding sequence (reviews, Cheney, 1992; Rhoads and Friedberg, 1997; Gillespie and Cyr, 2002,) the *Dictyostelium* talin actin-binding site (ABS), the *Rattus* MAP2 tubulin-binding site (TBS), and the Mus radixin FERM-dimerization sequence (FDS) were used to search for putative IQ, ABS, TBS, and FDS sites within Myo1, respectively. Modern DNA recombinant methods were used to PCR amplify Myo1-tail constructs and clone them into pIGF-1 (pIGF-1 figure). pIGF-1 was generously donated by Douglas Chalker. Restriction and polymerase enzymes were purchased from Promega (Madison, WI.), and primers (table 2) were purchased from Oligos Etc. (Wilsonville, OR.). Wild-type strain 428 *Tetrahymena thermophila* template DNA for PCR was isolated by the Stratagene DNA Isolation Kit (La Jolla, CA.). *MYO1* coding sequence was accessed from the NCBI database (accession code: U87268). Amplify3.1 (Bill Engels, 2005, University of Wisconsin) and Oligotech

(Oligos Etc.) software was used to design primers (Table 2). The MyTH4 coding region was synthetically engineered and cloned into pIGF-1.

	Primer Description	**Direction**	**Sequences**
GFP-Myo1 Tail constructs	1.362 kB *GFP-FERM* w/ Xho I site	Forward	5' → 3' ATACTCGAGAAAAGTGAGTAAATACAAAGAG GATGCATCC
	1.362 kB *GFP-FERM* w/ Apa I site	Reverse	5' → 3' TTATGGGCCCTCATTGACTTTTTTCTTATTATTG TTGTTAC
	1.053 kB *GFP-FERM-T1* w/ Xho I site	Forward	5' → 3' ATACTCGAGAAAAGTGAGTAAATACAAAGAG GATGCATCC
	1.053 kB *GFP-FERM-T1* w/ Apa I site	Reverse	5' → 3' TTTGGGGCCCTCATTCTTTAGAAGAAAGTGTGT CATTTAGT
	0.438 kB *GFP-FERM-T2* w/ Xho1 site	Forward	5' → 3' GAACTATACAAAAACCTCGAGTAAGCAAAGTT AGCCTACATAC
	0.438 kB *GFP-FERM-T2* region w/ApaI site	Reverse	5' → 3' GGTTGGTTGTTTGTTGGGCCCTCATTGACTTTT TTCTTATTATTG
Disruption Construction	5.656 kB MYO1a (4262 kB *MYO1*) w/ Acc65 I site	Forward	5' → 3' GTCGACAAGACAGTTG
	5656 kB MYO1a (4262 kB *MYO1*) w/ Sal I site	Reverse	5' → 3' GGTACCACAAACACTTC
	1575 kB MYO1b w/ Sac II site	Forward	5' → 3' CCGCGGTTTACGTTTA
	1575 kB MYO1b w/ Sac I site	Reverse	5' → 3' GAGCTCATTGACTTTTTTC

TABLE 2. List of Primers (restriction site sequences are underlined)

Creation of MyTH4 and FERM Expression Constructs.

Standard recombinant techniques were used to create a GFP (Green Fluorescent Protein)-tagged Myo1 MyTH4 (aa 1234-1376) construct by fusing 474 nucleotides of *MYO1* tail DNA sequence to the 3' of the GFP sequence. An in-frame TGA stop triplet was fused to the 3' of the 474 bp of Myo1 tail sequence. The 474 bp of *MYO1* tail sequence includes all of the MyTH4 domain (429 bp) and a spacer tail domain sequence of 33 bp at the 5' of MyTH4 and 12 bp of tail sequence at the 3' of MyTH4. Spacer sequences are transcribed and translated into 11 amino acids at the MyTH4 N-terminus and 4 amino acids at the MyTH4 C-terminus. The construct was cloned into an expression vector containing a metallothionein promoter, and the vector was used to transform *Tetrahymena* by biolistic bombardment. Similarly, a GFP-tagged Myo1-MyTH4 truncation (aa 1223-1343) construct, which eliminated a putative tubulin binding site, was created by fusing 360 nucleotides of *MYO1* tail DNA sequence to the 3' of the GFP sequence. An in-frame TGA stop triplet was fused to the 3' of the 360 bp of *MYO1* tail sequence. The 360 bp of *MYO1* tail sequence includes a 33 bp spacer at the 5' of MyTH4 and 327 bp of the MyTH4 sequence. The truncated Myo1-MyTH4 construct is transcribed and translated into the first 109 of the 143 amino acids in the Myo1-MyTH4 tail region preceded by an 11 amino acids N-terminus spacer. Similarly, a GFP-tagged Myo9-MyTH4 truncation (aa 1049-1226) constructed was created by fusing the genomic region of the MyTH4 region (bp 3145-3674) DNA to the 3' end of the GFP cassette. Each construct was separately cloned into an expression vector containing a methallothionein promoter, and each vector was used to transform *Tetrahymena thermophila*. The organization of Myo1 and the predicted GFP-fusion proteins are

diagrammed in Fig. 2. The expression vector (pIGF) was developed by Dr. Meng-Chao Yao, Institute of Molecular Biology, Taipei, Taiwan and kindly donated by Dr. Douglas Chalker.

Dimensions of Myo1 FERM (Fig. 1) are based on an alignment with *Mus* radixin FERM (not shown). Standard recombinant techniques were used to create tagged, truncated *MYO1* tail domains by fusing a GFP (Green Fluorescence Protein) sequence to the 5' end of three different regions of the *MYO1* tail domain (Fig. 1B). One truncation of the Myo1 tail domain (GFP-FERM) was created by fusing GFP to the last 1362 nucleotides in the *MYO1* tail (aa 1357-1809). Therefore, in GFP-FERM, the entire region N-terminal to the FERM domain was deleted. In another truncation (GFP-FERM-T1), GFP was fused to the 5' end of the first 1038 nucleotides in FERM (aa 1357-1686) followed by an inserted TGA stop triplet at the 3' end of the truncated FERM. For the third truncation (GFP-FERM-T2), GFP was fused to the 5' end of the last 438 nucleotides in the *MYO1* tail (aa 1675-1809). Each fused *MYO1* tail sequence was separately cloned into an expression vector containing a metallothionein promoter, and the vector was used to transform *Tetrahymena* by biolistic bombardment. The pIGF vector was developed by Dr. Meng-Chao Yao, Institute of Molecular Biology, Taipei, Taiwan and kindly donated by Dr. Douglas Chalker.

Creation of Replacement Construct:

Modern DNA recombinant techniques were used to create the replacement construct by independently PCR amplifying two different fragments of MYO1 and cloning them into sites that flank a disruption cassette. MYO1A is a 5667 bp region of MYO1 that includes the first 4262 bp coding sequence and 1399 bp leader sequence of

the MYO1 coding sequence was PCR amplified using forward 5'-GGTACCACAAACACTTC-3' and reverse 5'-GTCGACAAGACAGTTG-3' primers (Oligos etc., Wilsonville, OR), and cloned into PCR 2.1 (Invitrogen, Carlsbad, Ca). Similarly, MYO1B is a 1584 bp sequence of MYO1, 3' of MYO1A, that was PCR amplified using forward 5'-CCGCGGTTTACGTTTA 3' and reverse 5'-GAGCTCATTGACTTTTTTC-3' primers (Oligos etc), and cloned into PCR 2.1 (Invitrogen). MYO1A was cut with RE's *ACC65I* and *SalI* and MYO1B was cut with RE's *NotI* and *BamHI* and cloned flanking the disruption cassette in the pMrpl29B vector (kindly donated by Dr. Douglas Chalker). The disruption cassette is composed of a cycloheximide resistance gene that is under a metallothionein promoter and a transcriptional terminating sequence that directly flanks the 3' sequence of MYO1A. The replacement construct was designed to replace endogenous MYO1 in Tetrahymena by homologous recombination and transcribe a gene that is translated to express a truncated Myo1 (amino acids 1-1214) followed by a 6 amino acid spacer and a translational TGA stop triplet, and therefore will be missing all of the MyTH4/FERM domain.

Strains

Two *Tetrahymena* strains will be used in this study: wild type CU427 and CU428. Cells will be grown in Neff's (Orias et al., 2000) medium at 30^{o} C.

Antibodies

Anti-GFP and appropriate secondary antibodies will be purchased commercially. Anti-actin and anti-Myo1 are currently available in our lab from previous studies (Hosein et al., 2003; Hosein and Gavin, 2007).

Mating

Logarithmically growing cells in Neff's medium (Orias et al., 2000) will be concentrated by centrifugation, resuspended in 10 mM Tris-Cl (pH 7.4) to yield an optical density of 0.2 as measured at 540 nm, and they will be starved overnight at 30 degrees C. Mating will be initiated by mixing equal numbers of cells (approximately 5-ml total volume) in plastic 45-ml Petri dishes. Conjugal pairs will be formed from CU427 and CU428.

Biolistic Bombardment of Conjugating *Tetrahymena*

Biolistic bombardment was achieved with a Helios Gene Gun (Bio-Rad, Richmond, CA). The "bullets" were prepared with 1.0 µm gold particles according to the protocol described by Woods & Zito (2008). For gun shoots, a concentrated volume of *Tetrahymena* conjugal pairs (8-10 hours after mixing the mating types) were placed on 2.4 cm GF/A sterile Whatman filter paper in 100 x15 mm plastic Petri dishes. Cells were fired upon three consecutive times at pressures of 120 psi, 150 psi, and 180 psi. Seven ml of modified Neff's medium containing 1x antibiotic/antimycotic mix (Invitrogen, Carlsbad, CA) was added to the Petri dishes containing the bombarded cells, was incubated overnight at 30^{o} C. Bombarded cells were subsequently diluted with modified Neff's containing 100 µg/ ml paromomycin and 1x antibiotic/antimycotic mix. Two hundred fifty µl aliquots will be placed in Costar polypropylene cluster U-bottomed 96 well plates (Corning, Lowell, MA) and were incubated at 30^{o} C. Transformants were evident within 3-5 days.

Biolistic Bombardment of Conjugating *Tetrahymena*

Transformation of *Tetrahymena* with previously described constructs was achieved by biolistic bombardment (Cassidy-Hanley,D. 1997; Bruns,P J. 2000) of

conjugating *Tetrahymena* with the Bio-Rad (Hercules, CA) hand-held Helios Gene Gun by the following method. Wild type 427 and 428 *Tetrahymena* cells were grown at 30°C overnight, in bottles that contained 30 ml of modified Neff's media (Orias et al., 2000). Logarithmically growing cells were gently centrifuged washed three times, and resuspended in 30ml of 10 mM Tris-Cl (pH 7.40) to yield an optical density of 0.2 as measured at 540 nm, and starved overnight. The following day, approximately equal number of cells were mixed and allowed to mate. Conjugal pairs (8-10 hours after mixing) were concentrated by gentle centrifugation, placed on sterile 2.4 cm GF/A Whatman filter paper in 100 x 15 mm plastic Petri dishes, and were fired upon three consecutive times with fresh "bullets" at pressures of 120 psi, 150 psi, and 180 psi.

Preparation of "Bullets" and Use of Gene Gun.

The "bullets" consist of 1.0 micron DNA coated gold particles that were prepared by the following procedure adapted from the Woods and Zito (2008) protocol and the Bio-Rad handbook protocol.

1. Preparation of DNA

Fresh PolyVinylPyrolidone (PVP) ethanol suspension solution was prepared by adding 175 µL of 20mg/ml PVP solution in a sterile screw cap container, and the solution was diluted with fresh ethanol to make a final volume of 3.5ml (i.e. final concentration is 0.01mg/ml PVP). 50 µL of 200 proof ethanol was added to 50 µL of 0.10 spermidine in a microfuge tube containing 50 mg of 1.0 micron Gold (Au) particles and the mixture was sonicated and vortexed for 2-3 secs. 100 µg (100 µL) DNA, which was prepared by the Qiagen (Valencia, CA) HiSpeed Maxi Plasmid Prep Kit, was added to the gold & spermidine solution, and the mixture was gently sonicated. Drop-wise, 100µl of Calcium

Chloride (2.5M) was added to the mixture and sonicated for 2-3 minutes. The mixture was allowed to precipitate at room temperature for 10 min, and then briefly sonicated. The mixture was pulse-centrifuged for 15seconds, and the supernatant was removed and discarded. The mixture was resuspended in the remaining supernatant, and washed 3-times with 1ml fresh EtOH. After the final wash, repeated 200ul of PVP solution was used to transfer solution into freshly made PVP solution.

2. Coating the Plastic (From Bio-Rad protocol):

A ~ 30 inch tube was cut and dried in the tube prep station with Nitrogen at 0.35-0.4 Liters Per Minute(s) (LPM) for at least 15 minutes. The DNA coated gold mixture was inverted several times. Most of the mix was drawn and quickly transferred to the dried tube. The micro-carriers were allowed to settle for 3-5minutes. The solution was removed at a rate of 0.5-1.0"/ sec (the tube is emptied in within 30-45 secs). The tube was rotated 180 degrees and the gold was allowed to coat the inside of the tubing for 3-4 secs. The tubing prep station was turned on (I) to start rotating and the Gold to smeared the tubing for 20-30 second. The nitrogen valve was later opened to allow Nitrogen out at 0.35-.4LPM for 3-5 minutes. Finally, the rotator was turned off, and the nitrogen valve was closed.

3. Cutting the Tubing:

A vial with desiccant pellet inside was placed in the base of the tubing cutter (hole under the cutter). The tubing was inserted until it made contact with rear. The cutter was pressed down to cute DNA-coated, gold-smeared tube. Unused bullets were stored at 4°C in a tightly capped vial labeled, and wrapped in parafilm.

4. Using the Gun:

An empty cartridge holder was inserted into the Helios Gene Gun, and the gun was pressurized to fire at 200 ATM. Loaded bullets were loaded into the cartridge holder and were fired at unsuspecting *Tetrahymena*. Bombarded cells were incubated overnight at 30C and the diluted with modified Neff's containing 120 µg/ml paromomycin and 1x antibiotic/antimycotic mix. Two hundred fifty µL aliquots were placed in Corning (Lowell, MA) 96 well plates and incubated at 30°C. Transformants were evident within 3-5 days.

Verification of Replacement Construct:

Genomic DNA was extracted from wild type 428 and *MYO1* truncated replacement strains of *Tetrahymena thermophila* using the Stratagene DNA Isolation Kit (La Jolla, CA.) and were separately used as template for PCR reactions. Two primers (Eurofins, Huntsville, Al), forward 5'-AGCTATCTGAATTAGGAGAGTAGAAGC-3' and reverse 5'-CTACTGGTTGTTGGCAGTATGCTG-3' were used to verify the replacement of endogenous *MYO1*. The PCR product for wild type strains expressing endogenous *MYO1* was expected to be 1181 nucleotide bases. The PCR product for the replacement construct was expected to be 2489 nucleotide bases. The running condition for the PCR reaction was (94°C, 30 seconds; 62°C, 30 seconds; 72°C, 2:30 minutes; 30 cycles).

Expression of GFP-MyTH4

Transformed cells were grown for 8-12 hours at 30^{o}C prior to induction of GFP-MyTH4 expression by addition of 1.0 µg/ml $CdCl_2$. Cells were analyzed 6-12 hours after induction of GFP-MyTH4 expression.

Growth Curves

Spectrophotometer analysis at 540 nm was used to measure the growth rate of wild type and transformed *Tetrahymena*. Cells were grown in Neff's media supplemented with 0.1-0.5 µg/ml cadmium chloride at 30°C in 500 ml of culture medium contained in 2.8 liter Fernbach flasks.

Lysates

GFP-MyTH4 transformants were grown for two nights in 30 ml bottles of Neff's media at 30°C, and were treated to three hours of 1.0 µg/ml of $CdCl_2$ the next morning. However, GFP-FERM transformants cells were grown overnight in 30 ml bottles of Neff's media at 30°C. transformant cells were subsequently grown overnight in 0.5 µg/ml of $CdCl_2$ and incubated another night at 30°C. The cells were lysed with SDS according to the Hosein et al., 2003 protocol. To minimize protein degradation, Sigma-Aldrich protease inhibitors (St. Louis, MO) were added to the lysis buffer. Cells were concentrated and lysed by mixing with a solution consisting of 50 mM Tris-HCl (pH 8.0), 150 mM NaCl, 20 mM EDTA, 1% Na-deoxycholate, 1% Trition X-100 (Williams, 2000), and protease inhibitors (Turkewitz et al., 2000) for co-immunopreciptitation and low-speed sedimentation assays.

Immunoprecipitations

Lysates were treated with 1ml rabbit anti-actin serum (clone 7167) and incubated overnight at 4°C. One-milliliter of Protein A-agarose beads (Bio-Rad) was prepared by washing with Tris-Buffered Saline at pH 8.0 (TBS) until the OD_{280} was zero and resuspended in TBS for a total volume of ~1ml. Lysate and antiserum mixture was incubated with Protein A-agaorse beads for 2 hours in ice water with shaking. The

immunoprecipitate/Protein A-agarose beads mixture was washed again with TBS, until the OD_{280} was zero. Immuno-complexes were eluted with glycine at pH 3.0 from the beads and the eluate was immediately treated with 1.0M Tris-HCl (pH 8.0) to bring up the pH to 8.0. The same procedure as described for immune serum was completed with rabbit non-immune serum treatment with lysate for control experiments.

Affinity Purification with antiGFP-Agarose

Affinity resin was prepared by applying 400 µL of 100 µg/ml GFP polyclonal antibody (Invitrogen) to an NHS-Activated agarose spin column (33 mg capacity) (Pierce) and incubating at 4°C overnight. Unbound GFP-antibody was removed by centrifugation and the column was washed twice with phosphate buffered saline (PBS): 13.7 mM NaCl, 0.27 mM KCl, 10 mM Na_2HPO4, 0.2 mM KH_2PO4, pH 7.4. Agarose reactivity was quenched with 1.0 M ethanolamine (pH 7.4), and the quenched spin column was washed with PBS until OD at 280 was zero. Non-denatured, twice clarified, whole cell lysate from cells overexpressing GFP-MyTH4 was prepared as described for immunopreciptation and added to the spin column along with 10 mM Mg-ATP. The column was incubated overnight at 4°C overnight and subsequently washed with PBS until OD at 280 was zero. The column was eluted with 400 µL of 0.5 ml glycine (pH 3.0) and neutralized with 25 µL of 1.0 mM Tris (pH 8.0).

Electrophoresis

Lysates were separated on NuPage 4-12% Bis-Tris gels and stained with Novex colloidal blue from Invitrogen (Carlsbad, California) for gel analysis. Gels were electrophoretically transferred to PVDF membranes (Bio Rad) using standard methanol-based transfer protocols.

SDS-PAGE.

Transformed cells were grown overnight in Neff's medium at 30° C. Subsequently, $CdCl_2$ at a final concentration of 0.5 µg/ml was added to the culture, which was again incubated overnight at 30° C. Protocols for SDS-solubilized total cell lysate were previously described (Hosein et al., 2003). Polypeptides were separated on NuPage (Invitrogen) 4-12% Bis-Tris gels and stained with Coomassie Blue. Gel loadings were equal for all lysates.

Immunoblotting

Proteins were electrophoretically transferred to a PVDF membrane (Bio Rad) using standard methanol-based transfer protocols. Membranes were probed with appropriate antibodies in accordance with standard methods for immunoblotting. Immunoblots were developed with ECL Western Blotting Substrate (Pierce) and Biomax XAR film (Kodak).

Actin Filaments

Muscle F-actin (Cytoskeleton, Inc) was stabilized by treatment with 1.0 µM Alexa-Fluor 568-phalloidin (Invitrogen) in binding buffer (5.0mM Tris-HCl (pH 8.0), 0.2 mM $CaCl_2$, 2.0 mM $MgCl_2$, 5.0% glycerol).

Preparation of Microtubules

Tubulin and all other reagents for MT polymerization were purchased from Cytoskseleton, Inc (Denver, CO). Microtubules were polymerized from rhodamine labeled tubulin mixed with unlabeled tubulin (1:1) according to the manufacturer's protocol which is as follows: All reagents including labeled and unlabelled tubulin was thawed out. Sixty microliter of G-PEM solution was prepared by thorough mixing of 59.4

µl general tubulin buffer, and 0.6 µl 100mM of GTP. Four microliters of G-PEM solution and 1 µl of microtubule cushion buffer were added to rhodamine tubulin. Ten aliquots of unlabelled tubulin were prepared by adding 45 µl of G-PEM solution and 4.5 µl of Microtubule cushion buffer to unlabelled tubulin. Five micro liters of unlabeled tubulin solution was added to 5ul rhodamine-labeled tubulin to make a 1:1 ratio. The mixture was incubated at 35 °C for 25 minutes. Five-hundred micro-liters of General tubulin buffer was incubated at 35 °C for 15 minutes, followed by the addition 5 µl of taxol to tubulin buffer and the solution was stored at room-temperature. One hundred microliters of taxol-tubulin buffer was added to the tubulin after the 25-minute incubation period ended. The polymerized tubulin was observed by adding 1 µl of tubulin mixture in 20 µl of tubulin buffer-1x antifade mixture under confocal microscope.

Preparation of Whole Cell Extracts for Cosedimentation Assays

To prepare whole cell extracts, cells were washed free of culture medium and resuspended in extraction lysis buffer: 10 mM Tris pH 7.4, 20 mM KCl, 0.1 mM EGTA, 5 mM $MgCl_2$, 2 mM DTT, and 200 µl protease inhibitor/ml lysis buffer. The concentrated cell suspension was frozen at -20 °C for 10 minutes and subsequently thawed at room temperature, then put through a vigorous vortex and drawn up into a Pasteur pipette several times to lyse the cells. The lysate was clarified by centrifugation at 16,000 x *g* for 15 minutes. The supernatant was centrifuged a second time at 16,000 x *g* for 15 minutes. Supernatant from the second centrifugation was used in cosedimentation assays.

Cosedimentation Assays With GFP-MyTH4 IP

Phalloidin-stabilized F-actin (15 μM) in binding buffer containing 10 mM ATP was incubated with 160 μl of antiactin immunoprecipitation (IP) pellet for 15 minutes at 4°C followed by centrifugation at 16,000 x *g* for 15 minutes. The pellet was resuspended in 100 μl of actin-binding buffer and subsequently prepared for confocal microscopy. For microtubule cosedimentation assays 160 μl of antiactin GFP-MyTH4 IP were incubated with 3.5 μM taxol-stabilized microtubules in polymerization buffer for 15 minutes at 30°C followed by centrifugation at 16,000 x *g* for 15 minutes. The pellet was resuspended in 100 μl of binding buffer and used for confocal microscopy. For cosedimentation assays involving both F-actin and microtubules, 160 μl of antiactin GFP-MyTH4 IP were incubated with 3.5 μM taxol-stabilized microtubules in polymerization buffer for 15 minutes, and then 15 μM unlabeled F-actin in actin-binding buffer containing 10 mM ATP were added for another 15 minutes incubation.

Cosedimentation Assays With Whole Cell Extracts

For actin filament cosedimentation assays, stabilized F-actin (15 μM) was incubated with 160 μl of the cell lysate (with added 10 mM Mg-ATP) for 15 minutes at 4^0 C followed by centrifugation at 16,000 x *g* for 15 minutes. The pellet was resuspended in 100 μl of actin-binding buffer and subsequently prepared for confocal microscopy. For microtubule cosedimentation assays, 160 μl of whole cell lysate were incubated with 3.5 μM taxol-stabilized microtubules in polymerization buffer for 15 minutes at 30°C followed by centrifugation at 16,000 x *g* for 15 minutes. The pellet was resuspended in 100 μl of binding buffer and used for confocal microscopy. F-actin and microtubules were viewed from wet mounts sealed with nail polish.

Cosedimentation Assays with AntiGFP Pulldown Fraction

For actin filament cosedimentation assays, stabilized F-actin (15 μM) was incubated with 160 μl of antiGFP pulldown (with added 10 mM Mg-ATP) for 15 minutes at 4°C followed by centrifugation at 16,000 x *g* for 15 minutes. The pellet was resuspended in 100 μl of binding buffer and used for confocal microscopy For microtubule cosedimentation assays, 160 μl of antiGFP pulldown fraction were incubated with 3.5 μM taxol-stabilized microtubules in polymerization buffer for 15 minutes at 30^0 C followed by centrifugation at 16,000 x *g* for 15 minutes. The pellet was resuspended in 100 μl of binding buffer and used for confocal microscopy.

Confocal Microscopy of Living Cells

Living cells were embedded in a thin layer of 1.7 % low melting agarose on slide. Actin filaments and microtubules were viewed from wet mounts sealed with nail enamel. For observation of nuclei, DAPI (4', 6-diamidino-2-phenylindole, dihydrochloride) was used at a concentration of 10 μg/ml. Confocal microscopy was performed with a C-1 confocal system (Nikon, Inc., Melville, NY). A 60x 1.4 N.A. Nikon Apochromat oil immersion lens was used to capture images.

Isolation of Nuclei

To prepare a cell fraction enriched for nuclei, cells were washed free of culture medium and resuspended in extraction lysis buffer: 10 mM Tris pH 7.4, 20 mM KCl, 0.1 mM EGTA, 5 mM $MgCl_2$, 2 mM DTT, and 200 μl protease inhibitor (Sigma)/ ml lysis buffer. The concentrated cell suspension was frozen at -20°C degrees for 10 minutes and subsequently thawed at room temperature, then gently drawn up into a Pasteur pipette several times to lyse the cells without rupturing nuclear membranes. The extract was

centrifuged at 800 x *g* for 10 minutes. The supernatant was discarded; the pellet was resuspended in extraction buffer and centrifuged a second time at 800 x *g* for 10 minutes. The supernatant from the second centrifugation was discarded; the pellet, which contained intact nuclei, was resuspended in 100 µl extraction buffer and used for microscopy analysis.

Nocodazole

Cells overexpressing GFP-MyTH4 were given a 30 minute treatment with 30 mM nocodazole prior to fixation for immunofluorescence microscopy. Control cells received a 30-minute treatment with DMSO prior to processing for immunofluorescence microscopy.

Chapter 9. Closing Remarks

Replacement Construct for *MYO1*

A Replacement construct for *MYO1* was used to transform *Tetrahymena* with a truncated version of Myo1 that lacked MyTH4/FERM region of Myo1. PCR confirmed replacement of endogenous Myo1 gene, and immunoblot analysis showed stable expression of truncated Myo1 (not shown). However, complete phenotypic assortment for this gene was not achieved, as observed in PCR analysis and western blots, implying that Myo1 truncated for MyTH4/FERM is lethal to *Tetrahymena*.

Chapter 10 Bibliography

Adams, R. J., and Pollard T.D. (1986). Propulsion of organelles isolated from *Acanthamoeba* along actin filaments by myosin-I. *Nature, 322*(6081), 754-756.

Adams, R. J., and Pollard T.D. (1989). Binding of myosin I to membrane lipids. *Nature, 340*(6234), 565-568.

Allen RD. 1967. Fine structure, reconstitution, and possible functions of components of the cortex of *Tetrahymena pyrifoirmis*. *J Protozool* 14, 553-565.

Allen, R., & Wolf, R. (1979). Membrane recycling at the cytoproct of *Tetrahymena*. *Journal of Cell Science, 35*(1), 217-227.

Awan, A., Hamasaki, T., and Satir, P. (2004). Cloning and characterization of Kin5, a novel *Tetrahymena* ciliary kinesin II. *Cell Motility and the Cytoskeleton, 58*, 1-9.

Banga, I. (1942). The phosphatase activity of myosin. Stud. Inst. Med. *Chem. Univ*. Szeged. (I), 27–36.

Banga, I., and A. Szent-Györgyi. (1942). Preparation and properties of myosin A and B. Stud. Inst. Med. *Chem. Univ*. Szeged. (I), 5-15.

Barsoum, I.B., King-Smith, C., Myosin II and Rho kinase activity are required for melamosome aggregation in fish retinal pigment epithelial cells. (2007). *Cell Motility and the Cytoskeleton, 64,* 868-879

Basciano, P. A. & King-Smith, C. (2002) *Pigment Cell Res. 15* , 184–191.

Belyantseva, I.A., Boger, E.T., Naz, S., Frolenkov G.I., Sellers J.R., Ahmed Z.M., Griffith, A.J., and Friedman T.B. (2003). Myosin XVa localizes to the tips of inner ear sensory cell stereocilia and is essential for staircase formation of the hair bundle. *Proc Natl Acad Sci USA., 100*(24), 13958-13963.

Belyantseva, I.A., Boger, E.T., and Friedman T.B. (2005). Myosin-XVa is required for tip localization of whirlin and differential elongation of hair-cell stereocilia. *Nature Cell Biology, 7*, 148-156.

Berg JS, Derfler BH, Pennis CM, Corey DP, Cheney RE. 2000. Myosin-X, a novel myosin with pleckstrin homology domains, associates with regions of dynamic actin. *J Cell Sci* 113, 3439-3451.

Berg, J., Powell, B., & Cheney, R. (2001). A millennial myosin census. *Molecular Biology of the Cell, 12*(4), 780-794.

Blackburn, E. H. (1978). A tandemly repeated sequence at the termini of the extrachromosomal ribosomal RNA genes in tetrahymena. *Journal of Molecular Biology, 120*(1), 33-53.

Bleyman, L. K. (1992). Mapping the mating type locus of *Tetrahymena thermophila*: Meiotic linkage of mat to the ribosomal RNA gene. *Devel Genetics, 13*(1), 34-40.

Bohil, A. B., Robertson, B. W., & Cheney, R. E. (2006). Myosin-X is a molecular motor that functions in filopodia formation. *PNAS USA, 103*(33), 12411-12416.

Breshears LM, Wessels D, Soll DR, Titus MA. 2010. An unconventional myosin required for cell polarization and chemotaxis. *PNAS* USA 107, 6918-6923.

Bretscher A, Edwards K, Fehon RG. 2002 ERM proteins and merlin: integrators at the cell cortex. *Nat Rev Mol Cell Biol*., 3, 586-599.

Bretscher, A., Reczek, D., & Berryman, M. (1997). Ezrin: A protein requiring conformational activation to link microfilaments to the plasma membrane in the assembly of cell surface structures. *Journal of Cell Science, 110*(24), 3011-3018.

Bruns, P.J. (1986). Genetic organization of Tetrahymena. In: Gall, L. G. (ed.), *TheMolecular Biology of Ciliated Protozoa.* Academic Press, Orlando. p. 27-44.

Bruns, P. J., and Cassidy-Hanley, D. (2000). Biolistic transformation of macro- and micronuclei. In: Asai, D.J., and Forney, J.D. (ed), *Tetrahymena thermophila. Methods in Cell Biology, V(62).* Academic Press, San Diego. p. 501-512.

Brzeska, H., Lynch, T., & Korn, E. (1988). Localization of the actin-binding sites of acanthamoeba myosin IB and effect of limited proteolysis on its actin-activated Mg2+-ATPase activity. *Journal of Biological Chemistry, 263*(1), 427-435.

Cassidy-Hanley, D., Bowen, J., Lee, J. H., Cole, E., VerPlank, L. A., Gaertig, J., Gorovsky, M.A. and Bruns, P.J. (1997). Germline and somatic transformation of mating tetrahymena thermophila by particle bombardment. *Genetics, 146*,135-47.

Cao, T.T., Chang, W., Masters, S.E., and Mooseker M.S., (2004). Myosin-Va Binds to and Mechanochemically Couples Microtubules to Actin Filaments. *MBC., 15(1),* 151-161.

Chambers DN, Bretscher A. 2005. Ezrin mutants affecting dimerization and activation. *Biochemistry* 44, 3926-3932.

Cech, T.R. 1986 . A model for the RNA-catalyzed replication of RNA. *Proc Natl Acad Sci USA., 83*(12), 4360-4363.

Chasey, D., (1969). Observations on the Central Pair of Microtubules from the Cilia of Tetrahymena Pyriformis. *Journal of Cell Science, (5),* 453-458.

Chaparro-Olaya J, Margos G, Coles DJ, Dluzewski AR, Mitchell GH, Wasserman MM, Pinder JC. 2005. *Plasmodium falciparum* myosins: transcription and translation during asexual parasite development. *Cell Motil Cytoskel* 60, 200-213.

Chen, Z.Y., Hasson, T., Kelley, P.M., Schwender, B.J., Schwartz, M.F., Ramakrishnan, M., Kimberling, W.J., Mooseker M.S., and Corey, D.P. (1996). Molecular cloning and domain structure of human myosin-VIIa, the gene product defective in usher syndrome 1B. *Genomics, 36*(3), 440-448.

Cheney, R. E. and Mooseker M.S. (1992). Unconventional myosins. *Current Opinion in Cell Biology, 4*(1), 27-35.

Chishti AH, Kim AC, Marfatia SM, Lutchman M, Hanspal M, Jindal H, Liu SC, Low PS, Rouleau GA, Mohandas N, and others. 1998. The FERM domain: a unique module involved in the linkage of cytoplasmic proteins to the membrane. *Trends Biochem Sci,* 23, 281-282.

Chuang, C., Carpenter, A., Fuchsova, B., Johnson, T., deLanerolle, P., and Belmont, A. (2006). Long-range directional movement of an interphase chromosome site. *Current Biology, 16*(8), 825-831.

Cleffmann G. 1980. Chromatin elimination and the genetic organisation of the macronucleus in *Tetrahymena thermophila*. *Chromosoma*. 78, 313-325.

Conboy, J., Kan Y.W., Shohet, S.B., Mohandas N. (1986). Molecular cloning of protein 4.1, a major structural element of the human erythrocyte membrane skeleton. *Proc Natl Acad Sci USA.,*

Coluccio LM. 2008. Myosins: A Superfamily of Molecular Motors (Proteins and Cell Regulation). New York: Springer, 469pp.

Correas I., Padilla R., and Avila J., (1990). The tubulin-binding sequence of brain microtubule-associated proteins, tau and MAP-2, is also involved in actin binding. *Biochem J. 269(1),* 61–64.

Coue, M., Brenner, S.L., Spector, I., Korn, E.D. (1987). Inhibition of actin polymerization by latrunculin A. *FEBS Letters 213(2),* 316-318.

Diakowski, W. (2006). Protein 4.1, a component of the erythrocyte membrane skeleton and its related homologue proteins forming the protein 4.1/FERM superfamily. *Folia Histochemica Et Cytobiologica, 44*(4), 231-248.

Doberstein, S., and Pollard, T. (1992). Localization and specificity of the phospholipid and actin binding sites on the tail of acanthamoeba myosin IC. *The Journal of Cell Biology, 117*(6), 1241-1249.

Doll T., Meichsner M., Riederer B.M., Honegger P., and Matus A. (1993). An isoform of microtubule-associated protein 2 (MAP2) containing four repeats of the tubulin-binding motif. *Journal of Cell Science, 106(2),* 633-639.

Durbach A., Collins K., Matsudaira, R., Louvard, D., Coudrier, E. (1996). Brush border myosin-I truncated in the motor domain impairs the distribution and the function of endocytic compartments in an hepatoma cell line. *Proc Natl Acad Sci USA* 93(14) 7053-7058

Eisen, J.A., Coyne, R.S., Wu, M., Wu, D., Thiagarajan, M., Wortman, J.R., Badger, J.H., Ren, Q., Amedeo, P., Jones, K.M., Tallon, L.J., Delcher, A.L., Salzberg, S.L., Silva, J.C., Haas, B.J., Majoros, W.H., Farzad, M., Carlton, J.M., Smith, R.K. Jr., Garg, J., Pearlman, R.E., Karrer, K.M., Sun, L., Manning, G., Elde, N.C., Turkewitz, A.P., Asai, D.J., Wilkes, D.E., Wang, Y., Cai, H., Collins, K., Stewart, B.A., Lee, S.R., Wilamowska, K., Weinberg, Z., Ruzzo, W.L., Wloga, D., Gaertig, J., Frankel, J., Tsao, C.C., Gorovsky, M.A., Keeling, P.J., Waller, R.F., Patron, N.J., Cherry, J.M., Stover, N.A., Krieger, C.J., del Toro, C., Ryder, H.F., Williamson, S.C., Barbeau, R.A., Hamilton, E.P., Orias, E. (2006). Macronuclear genome sequence of the ciliate Tetrahymena thermophila, a model eukaryote. *PLoS biology.* 4(9)

Elde, N. C., Morgan, G., Winey, M., Sperling, L. and Turkewitz, A. P. (2005). Elucidation of clathrin-mediated endocytosis in tetrahymena reveals an evolutionarily convergent recruitment of dynamin. PLoS Genet. 1(52), 524-522.

Engelhardt, V. A., and Lyubimowa, M. N. (1939). Myosin and adenosinetriphosphatase. *Nature, 144*, 668-669.

Etournay, R., Zwaenepoel, I., Perfettini, I., Legrain, P., Petit, C., & El-Amraoui, A. (2007). Shroom2, a myosin-VIIa- and actin-binding protein, directly interacts with ZO-1 at tight junctions. *Journal of Cell Science, 120*(16), 2838-2850.

Flickinger, C. J. (1965). The fine structure of the nuclei of *Tetrahymena pyriformis* throughout the cell cycle. *The Journal of Cell Biology, 27*(3), 519-529.

Finnerty CM, Chambers D, Ingraffea J, Faber HR, Karplus PA, Bretscher A. 2004. The EBP50-moesin interaction involves a binding site regulated by direct masking on the FERM domain. *J Cell Sci.* 117, 1547-1552.

Foth, B., Goedecke, M., and Soldati, D. (2006). From the cover: New insights into myosin evolution and classification. *Proc Natl Acad Sci., 103*(10), 3681-3686.

Fujiu K, Numata, O. 2000 Reorganization of microtubules in the amitotically dividing macronucleus of *Tetrahymena. Cell Motil. Cytoskeleton,* 46, 17-27.

Fukui, Y. (1989). Myosin I is located at the leading edges of locomoting *Dictyostelium amoebae*. *Nature, 341*(6240), 328-331.

Gaertig, J., Gu, L., Hai, B., and Gorovsky M.A. (1994). High frequency vector-mediated transformation and gene replacement in tetrahymena. *Nucleic Acids Research, 22*, 5391-5398.

Garces. J. A. & Gavin, R. H. 1996. Identification of a myosin heavy chain gene *(TETMYO-1*) in *Tetrahymena. Mol. Bio. Cell 7(37),* 869-881.

Garcés, J. and Gavin R.H., (1998). A PCR screen identifies a novel, unconventional myosin heavy chain gene (MYO1) in tetrahymena thermophila. *The Journal of Eukaryotic Microbiology, 45*(3), 252-259.

Gavin, R. H. (1980). The oral apparatus of tetrahymena. V. oral apparatus polypeptides and their distribution. *Journal of Cell Science, 44*(1), 317-333.

Gavin, R. H. (1997). Microtubule-Microfilament Synergy in the Cytoskeleton. In: *Int Rev Cytol*, (173). New York, Academic Press. p. 207-242.

Gavin R.H. (1999) Synergy of cytoskeleton components. *BioScience, 49(8)*, 641-655.

Gavin, R. H. (2001). Myosins in protists. In: *Int Rev Cytol*, (206). New York, Academic Press. p. 97-134.

Gillespie, P., and Cyr, J. (2002). Calmodulin binding to recombinant myosin-1c and myosin-1c IQ peptides. *BMC Biochemistry 3(1),* 31-48.

Gotesman M, Hosein RE, Gavin RH. 2010. A FERM domain in a class XIV myosin interacts with actin and tubulin and localizes to the cytoskeleton, phagosomes, and nucleus in *Tetrahymena thermophila.* Cytoskeleton 67:90-101.

Greider, C. W. (1985). Identification of a specific telomere terminal transferase activity in *Tetrahymena* extracts. *Cell, 43*(2 Pt 1), 405-413.

Griffith L.M. and Pollard T.D. (1978). Evidence for actin filament-microtubule interaction mediated by microtubule-associated proteins. *JCB, (78),* 958-965.

Guerra, C., Wada, Y., Leick, V., Bell, A., and Satir, P. (2003). Cloning, localization, and axonemal function of tetrahymena centrin. *Molecular Biology of the Cell, 14*(1), 251-261.

Halliburton W.D., (1887). On muscle-plasma. *J Physiol (8),* 11-202.

Hamada K, Shimizu T, Matsui T, Tsukita S, Hakoshima T. 2000. Structural basis of the membrane-targeting and unmasking mechanisms of the radixin FERM domain. EMBO J. 19: 4449-4462.

Hamada K, Shimizu T, Yonemura S, Tsukita S, Tsukita S, Hakoshima T. 2003. Structural basis of adhesion-molecule recognition by ERM proteins revealed by the crystal structure of the radixin-ICAM-2 complex. *EMBO J,* 22, 502-514.

Hammonda JW, Caia D, Verhey KJ. 2008. Tubulin modifications and their cellular functions. Curr Opin Cell Biol 20:71-76.

Hasson, T., Gillespie, P.G., Garcia, D.J.A., MacDonald, R.B., Zhao Y.D., Yee D.A.G., Mooseker M.S., Corey D.P. (1997). Unconventional myosins in inner-ear sensory epithelia. *The Journal of Cell Biology, 137*(6), 1287-1307.

Hirono, M., Nakamura, M., Tsunemoto, M., Yasuda, T., Ohba, H., Numata, O. and Watanabe, Y. (1987). *Tetrahymena* actin: Localization and possible biological roles of actin in *Tetrahymena* cells. *J. Biochem*. *102*, 537-545.

Hoffmann, E.K., Rasmussen, L., and Zeuthen, E. (1974). Cytochalasin B: Aspects of Phagocytosis in Nutrient Uptake in *Tetrahymena*. *J Cell Sci. 15*, 403-406.

Hoey JG, Gavin RH. 1992. Localization of actin in the *Tetrahymena* basal body cage complex. *J Cell Sci* ,103, 629-641.

Horowitz S, Gorovsky MA. 1985. An unusual genetic code in nunclear genes of *Tetrahymena*. *Proc Natl Acad Sci,* 82, 2452-2455.

Hosein, R. E., Williams, S.A., and Gavin, R.H. (2005). Directed motility of phagosomes in *Tetrahymena thermophila* requires actin and Myo1p, a novel unconventional myosin. *Cell Motility and the Cytoskeleton, 61*(1), 49-60.

Hosein, R. E., and Gavin R.H. (2007). Myo1 localizes to phagosomes, some of which traffic to the nucleus in a Myo1-dependent manner in *Tetrahymena thermophila*. *Cell Motility and the Cytoskeleton, 64*(12), 926-937.

Huang, S., Jagadeeswaran, R., Liu, E. S., and Benz, E. J., Jr. (2004). Protein 4.1R, a microtubule-associated protein involved in microtubule aster assembly in mammalian mitotic extract. *Journal of Biological Chemistry, 279*(33), 34595-34602.

Hulo N., Bairoch A., Bulliard V., Cerutti L., Cuche B., De Castro E., Lachaize C., Langendijk-Genevaux P.S., and Sigrist C.J.A. (2008). The 20 years of PROSITE. *Nucleic Acids Res*. PS,=D245-D249.

Huxley, A. F. (1954). Structural changes in muscle during contraction interference microscopy of living muscle fibres. *Nature, 173*(4412), 971-973.

Jacobs, M. E., DeSouza, L. V., Samaranayake, H., Pearlman, R. E., Siu, K. W. M., and Klobutcher, L. A. (2006). The *Tetrahymena thermophila* phagosome proteome. *Eukaryotic Cell, 5*(12), 1990-2000.

Katijama, Y., and Thompson, G.A. Jr., (1977). Differentiation of Food Vacuolar Membranes During Endocytosis in *Tetrahymena*. *Journal of Cell Biology*, 75, 436-445.

Kiehart, D.P., Franke J.D., Chee M.K., Montague R.A., Chen T.L., Roote J., and Ashburner M. (2004). *Drosophila* crinkled, Mutations of Which Disrupt Morphogenesis and Cause Lethality, Encodes Fly Myosin VIIA. *Genetics, 168,* 1337-1352.

Kitano K, Yusa F, Hakoshim T. 2006. Structure of dimerized radixin FERM domain suggests a novel masking motif in C-terminal residues 295–304. Acta Crystallogr *Sect F Struct Biol Cryst Commun.*, 62, 340–345.

Langford G.M. (1995). Actin- and microtubule-dependent organelle motors: interrelationships between the two motility systems. *Curr Opin Cell Biol. (1)*, 82-88.

Lee HS, Bellin RM., Walke DL, Patel B, Powers P, Liu H, Garcia-Alvarez B, de Pereda JM, Liddington RC, Volkmann N, Hanein D, Critchley DR, Robson, RM. 2004. Characterization of an actin-binding site within the talin FERM domain. *J. Mol Biol* 343, 771-784.

Lee, H. Bellin, R.B., Walker, D.L., Patel B., Powers, P., Liu, Garcia-Alverz, B., Pereda, J.M.D., Liddington, R.C., Volkmann, N., Hamein, D., Critchley, D.R., and Robson, M. (2004). Characterization of an actin-binding site within the talin FERM domain. *Journal of Molecular Biology, 343*(3), 771-784.

Lee, W., Ostap, E. M., Zot, H. G., and Pollard, T. D. (1999). Organization and ligand binding properties of the tail of acanthamoeba myosin-IA. Identification of an actin-binding site in the basic (Tail Homology-1) domain. *Journal of Biological Chemistry, 274*(49), 35159-35171.

Lengsfeld A.M., Löw, I., Wieland, T., Dancker, P., and Hasselbach W. (1974). Interaction of Phalloidin with Actin. *Proc Natl Acad Sci 71(7)*, 2803–2807.

Lewis S.A., Wang D.H., and Cowan N.J. (1988). Microtubule-associated protein MAP2 shares a microtubule binding motif with tau protein. *Science 242(4880)*, 936-939

Li Q, Nance MR, Kulikauskas R, Nyberg K, Fehon R, Karplus PA, Bretscher A, Tesmer JJ. 2006. Self-masking in an intact ERM-merlin protein: an active role for the central alpha-helical domain. *J Mol Biol.,* 365, 1446-1459.

Liu, R., Woolner, S., Johndrow, J. E., Metzger, D., Flores, A. and Parkhurst, S. M. (2008). Sisyphus, the Drosophilamyosin XV homolog, traffics within filopodia transporting key sensory and adhesion cargos. *Development,* 135, 53-63.

Lu, Q., and Henderson E. (2000). Two tetrahymena G-DNA-binding proteins, TGP1 and TGP3, share novel motifs and may play a role in micronuclear division. *Nucleic Acids Research, 28*(15), 2993-3001.

Lymn, R.W., and Taylor E.W. (1971). Mechanism of adenosine triphosphate hydrolysis by actomyosin. *Biochemistry, 10*(25), 4617-4624.

Mattagajasingh, S.N., Huang, S.C., Hartenstein, J.S., and Benz E.J. (2000). Characterization of the interaction between protein 4.1 R and ZO-2. A possible link between the tight junction and the actin cytoskeleton. *The Journal of Biological Chemistry, 275*(39), 30573-30585.

McNeil, E. L., Tacelosky, D., Basciano, P., Biallas, B., Williams, R., Damiani, P., Deacon, S., Fox, C., Stewart, B., Petruzzi, N., Osborn, C., Klinger, K., Sellers, J. R., and Smith, C. K. (2004) *Cell Motil. Cytoskeleton*, 58, 71-82

Muranen T., Grönholm M., Lampin A., Lallemand D., Zhao F., Giovannini M., and Carpén O. (2007). The tumor suppressor merlin interacts with microtubules and modulates Schwann cell microtubule cytoskeleton. *Hum Mol Genet., 16(14),* 1742-1751.

Nanney, D. L., and McCoy, J.W. Characterization of the Species of the *Tetrahymena pyriformis* Complex. *Transactions of the American Microscopical Society*, 95(4) 664-682

Narasimhulu, S. B. (1998). Characterization of microtubule binding domains in the *Arabidopsis* kinesin-like calmodulin binding protein. *The Plant Cell, 10*(6), 957-966.

Niggli V, Andreoli C, Roy C, Mangeat P. 1995. Identification of a phosphatidylinositol-4,5-bisphosphate-binding domain in the N-terminal region of ezrin. *FEBS Lett.,* 376, 172-176.

Nilsson, J.R., Van Deurs, B. (1983). Coated pits and pinocytosis in Tetrahymena. *J Cell Sci. 63*, 209– 222

Ng S.F., (1978). Directionality of microtubule assembly: an in vivo study with the ciliate *Tetrahymena*. *J Cell Sci 33(1),* 227-234

Numata O., Fujiu K., and Gonda K. (1999). Macronuclear division and cytokinesis in *Tetrahymena*. *Cell Biology International, 23*(12), 849-857.

Odronitz F. and Kollmar M. (2007). Drawing the tree of eukaryotic life based on the analysis of 2,260 manually annotated myosins from 328 species. *Genome Biology,* 8 (9). 10.1186/gb-2007-8-9-r196

Orias, E. (1991). On the evolution of the karyorelict ciliate life cycle: Heterophasic ciliates and the origin of ciliate binary fission. *Bio Systems, 25*(1-2), 67-73.

Orias E. Flacks M. 1975. Macronuclear genetics of *Tetrahymena*. I. Random distribution of macronuclear genecopies in *Tetrahymena pyriformis* syngen 1. *Genetics,* 79, 187-206.

Orias E, Hamilton EP, Orias J. 2000. *Tetrahymena* as a laboratory organism: Useful strains, cell culture, and cell line maintenance. In: Asai DJ, Forney JD, editors. Methods in Cell Biology: *Tetrahymena thermophila*. New York: Academic Press 62: 189-211.

Percipalle P, Fomproix N, Cavellán E, Voit R, Reimer G, Krüger T, Thyberg J, Scheer U, Grummt I, Farrants AK. 2006. The chromatin remodelling complex WSTF-SNF2h interacts with nuclear myosin 1 and has a role in RNA polymerase I transcription. *EMBO Rep*. 5:525-30

Pearson M.A., Reczek D., Bretscher A., and Karplus P.A. (2000). Structure of the ERM protein moesin reveals the FERM domain fold masked by an extended actin binding tail domain. *Cell.*, *101*(3), 259-270

Pérez-Ferreiro, C. M. (2006). Protein 4.1R self-association: Identification of the binding domain. *The Biochemical Journal, 400*(3), 457.

Philimonenko VV, Janácek J, Harata M, Hozák P. (2010). Transcription-dependent rearrangements of actin and nuclear myosin I in the nucleolus. Histochem Cell Biol. 134(3):243-9

Pollard, T. D., and Korn, E. D. (1973). Acanthamoeba myosin. I. Isolation from *Acanthamoeba castellanii* of an enzyme similar to muscle. *Journal of Biological Chemistry, 248*(13), 4682-4690.

Pollenz, R. S. (1992). The dictyostelium essential light chain is required for myosin function. *Cell, 69*(6), 951-962.

Pranchevicius MC, Baqui MM, Ishikawa-Ankerhold HC, Lourenço EV, Leão RM, Banzi SR, dos Santos CT, Roque-Barreira MC, Espreafico EM, Larson RE. (2008). Myosin Va phosphorylated on Ser1650 is found in nuclear speckles and redistributes to nucleoli upon inhibition of transcription. CMC. 65(6): 441-56.

Rannestad J., and Williams N.E., The synthesis of microtubules and other proteins of the oral apparatus in *Tetrahymena pyriformis*. *JCB 50*, 709-720,

Rahaman A, Elde NC, Turkewitz AP. 2008. A dynamin-related protein required for nuclear remodeling in *Tetrahymena*. *Curr Biol*., 18, 1227-1233.

Rasmussen, L., and Orias, E. (1975). Tetrahymena: Growth Without Phagocytosis. *Science, 190*(4213), 464-465.

Rhoads, A.R., Friedberg, F. (1997). Sequence motifs for calmodulin recognition. *The FASEB Journal, 11*(5), 331-340.

Richards, T.A. and Cavalier-Smith, T. (2005). Myosin domain evolution and the primary divergence of eukaryotes. *Nature, 436*(7054), 1113-1118.

Reddy, V.S., and Reddy A.S., (1999). A plant calmodulin-binding motor is part kinesin and part myosin. *Bioinformatics, 15*(12), 1055-1057.

Saitoh A, Takiguchi K, Tanaka Y, Hotani H. 1998. Opening-up of liposomal membranes by talin. *Proc Natl Acad Sci USA* 95, 1026-1031.

Salerno VP, Calliari A, Provance DW Jr, Sotelo-Silveira JR, Sotelo JR, Mercer JA. (2008). Myosin-Va mediates RNA distribution in primary fibroblasts from multiple organs. CMC. 65(5):422-33.

Sandquist, J.C., Bement, W., (2010). Characterizing the Role of Myosin-10 in Regulating Mitotic Spindle Structure and Function. *Mol. Biol. Cell 21 (suppl),* Abstract B 1263.

Sandquist, J.C., Woolner, s., Bement, W., (2009). Characterization of a Novel Interaction between Myosin-10 and a Mitotic Kinase. *Mol. Biol. Cell 20 (suppl),* Abstract B 513.

Shearer, A.E., Hildebrand, M.S., Webster, J.A., Kahrizi, K., Meyer, N.C., Jalalvand, K., Arzhanginy, S.,Kimberling, W.J., Stephan, D., Bahlo, M., Smith, R.J. and Najmabadi, H. 2009. Mutations in the first MyTH4 domain of MYO15A are a common cause of DFNB3 hearing loss. *Laryngoscope* 119, 727-733.

Stattilaro R.F., Dentler W.L., and LeCluyse E.L. (1981). Microtubule-associated proteins (MAPs) and the organization of actin filaments in vitro. *JCB, (90),* 467-473.

Schwander M, Lopes V, Sczaniecka A, Gibbs D, Lillo C, Delano D, Tarantino LM, Wiltshire T, Williams DS, Müller U. (2009). A novel allele of myosin VIIa reveals a critical function for the C-terminal FERM domain for melanosome transport in retinal pigment epithelial cells. J Neurosci. 29(50):15810-8.

Straub, F.B. (1942). Actin. Stud. Inst. Med. *Chem. Univ*. Szeged. II:3–15.

Straub, F.B. (1943). Actin, II. Stud. Inst. Med. *Chem. Univ*. Szeged. III:23–37.

Shang, Y., Song, X., Bowen, J., Corstanje, R., Gao, Y., Gaertig, J., Gorovsky M.A. (2002). A robust inducible-repressible promoter greatly facilitates gene knockouts, conditional expression, and overexpression of homologous and heterologous genes in *Tetrahymena thermophila. PNAS, 99*(6), 3734-3739.

Shimizu T., Seto A., Maita N., Hamada K., Tsukita S., Tsukita S., and Hakoshima T. (2002). Structural basis for neurofibromatosis type 2. Crystal structure of the merlin FERM domain. *J Biol Chem. 277*(12):10332-10336

Smith JS, Yakisich JS, Kapler GM, Cole ES, Romero P. 2004. A ß-Tubulin mutation selectively uncouples nuclear division and cytokinesis in *Tetrahymena thermophila*. *Eukaryot. Cell,* 3, 1217-1226.

Spudich J.A., Lin S., (1973). Cytochalasin B, Its Interaction with Actin and Actomyosin from Muscle. *Proc Natl Acad Sci., 9(2),* 442–446.

Stuart KS, Cole, ES 2000. Nuclear and cytoskeletal fluorescence microscopy techniques. In: Asai, DJ, Forney JD, editors. Methods in Cell Biology: *Tetrahymena thermophila*. New York: Academic Press 62: 291-311.

Sugita, M., Nakano, K., Sato, M., Toyooka, K. and Numata, O. (2009) The roles of actin cytoskeleton and microtubules for membrane recycling of a food vacuole in *Tetrahymena thermophila*. *Cell Motil Cytoskeleton*, 66: 371-377.

Takeda S, Saitoh A, Furuta M, Satomi N, Ishino A, Nishida G, Sudo H, Hotani H, Takiguchi K. 2006. Opening of holes in liposomal membranes is induced by proteins possessing the FERM domain. J Mol Biol. 362:403-413

Titus MA. 2003. An unconventional myosin essential for the initiation of *Dictyostelium* development. Mol Biol Cell 14:S, 181a.

Todi, S.V., Sivan-Loukianova, E., Jacobs J.S., Kiehart, D.P., and Eberl, D.F. (2008). Myosin VIIA, important for human auditory function, is necessary for drosophila auditory organ development. *PloS One, 3*(5) :e2115.

Tondravi M.M., and Yao M.C., (1986). Transformation of *Tetrahymena thermophila* by microinjection of ribosomal RNA genes. *PNAS 83*, 4369-4373.

Tuxworth, R. I., Stephens, S., Ryan, Z. C., and Titus, M. A. (2005). Identification of a myosin VII-talin complex. *Journal of Biological Chemistry, 280*(28), 26557-26564.

Wang A, Liang Y, Fridell RA, Probst FJ, Wilcox ER, Touchman JW, Morton CC, Morell RJ, Noben-Trauth K, Camper SA, Friedman TB.1998. Association of unconventional myosin MYO15 mutations with human nonsyndromic deafness DFNB3. *Science,* 280, 1447-1451.

Weber, K. L. (2004). A microtubule-binding myosin required for nuclear anchoring and spindle assembly. *Nature, 431*(7006), 325-329.

Weil D, Blanchard S, Kaplan J, Guilford P, Gibson F, Walsh J, Mburu P, Varela A, Levilliers J, Weston MD, et al. 1995. Defective myosin VIIA gene responsible for Usher syndrome type 1B. *Nature,* 374, 60-61.

Williams NE. 2000. Immunoprecipitation Procedures. In: Asai DJ, Forney JD, editors. Methods in Cell Biology: *Tetrahymena thermophila*. New York: Academic Press 62:449-453

Williams, N., and Williams, R. (1976). Macronuclear division with and without microtubules in tetrahymena. *Journal of Cell Science, 20*(1), 61-77.

Williams, N.E., Tsao, C.C., Bowen, J., Hehman, G.L., Williams R.J., and Frankel J. (2006). The Actin Gene ACT1 Is Required for Phagocytosis, Motility, and Cell Separation of *Tetrahymena thermophila*. *Eukaryotic Cell 5(3),* 555-567.

Williams, S. A., Hosein R.E. and Gavin R.H. (2000). MYO1, a novel, unconventional myosin gene affects endocytosis and macronuclear elongation in tetrahymena thermophila. *The Journal of Eukaryotic Microbiology, 47*(6), 561-568.

Williams, S. A., and Gavin, R.H. (2005). Myosin genes in tetrahymena. *Cell Motility and the Cytoskeleton, 61*(4), 237-243.

Wloga D, Rogowski K, Sharma N, Van Dijk J, Janke C, Eddé B, Bré MH, Levilliers N, Redeker V, Duan J, Gorovsky MA, Jerka-Dziadosz M, Gaertig J. 2008. Glutamylation on alpha-tubulin is not essential but affects the assembly and functions of a subset of microtubules in *Tetrahymena thermophila*. *Eukaryot Cell* 7, 1362-1372.

Wolfrum, U., Liu, X., Schmitt, A., Udovichenko, I.P., Williams, D.S. (1998). Myosin VIIa as a common component of cilia and microvilli. *Cell Motility and the Cytoskeleton, 40*(3), 261-271.

Woods G., and Zito K. (2008). Preparation of Gene Gun Bullets and Biolistic Transfection of Neurons in Slice Culture. *JoVE*. 12. http://www.jove.com/index/Details.stp?ID=675, doi: 10.3791/675

Xu, H. and Gutman, D. H. (1998) Merlin differentially associates with the microtubule and actin cytoskeleton. *J. Neurosci. Res. 51*, 403–415

Xu, P., Mitchelhill, K. I., Kobe, B., Kemp, B. E., and Zot, H. G. (1997). The myosin-I binding protein Acan125 binds the SH3 domain and belongs to the superfamily of leucine-rich repeat proteins. *PNAS, 94*(8), 3685-3690.

Yan, B., Calderwood, D. A., Yaspan, B., and Ginsberg, M. H. (2001). Calpain cleavage promotes talin binding to the beta 3 integrin cytoplasmic domain. *Journal of Biological Chemistry, 276*(30), 28164-28170.

Yang Y, Baboolal TG, Siththanandan V, Chen M, Walker ML, Knight PJ, Peckham M, Sellers JR. 2009. A FERM domain autoregulates *Drosophila* myosin 7a activity. *Proc Natl Acad Sci USA* 106, 4189-4194.

Yao, M. C. (1986). Amplification of Ribosomal RNA genes. In: Gall, L. G. (ed.), *The Molecular Biology of Ciliated Protozoa.* Academic Press, Orlando. p. 179-201.

Yonezawa, S., Yoshizaki, N., Sano, M., Hanai, A., Masaki, S., Takizawa, T., Kageyama, T., Moriyama, A. (2003). Possible involvement of myosin-X in intercellular adhesion: Importance of serial pleckstrin homology regions for intracellular localization. *Development, Growth Differentiation, 45*(2), 175-185.

Yumura, S., and Uyeda, T.Q. (1997). Transport of myosin II to the equatorial region without its own motor activity in mitotic *Dictyostelium* cells. *Molecular Biology of the Cell, 8*(10), 20890-2099.

Zaug, A., and Cech, T. (1986). The intervening sequence RNA of tetrahymena is an enzyme. *Science, 231*(4737), 470-475.

Zhang H, Berg JS, Li Z, Wang Y, Lang P, Sousa AD, Bhaskar A, Cheney RE, Stromblad S. 2004. Myosin-X provides a motor-based link between integrins and the cytoskeleton. *Nat Cell Biol.,* 6, 523-531.